# Extreme Compound and Seesaw Hydrometeorological Events in New Zealand: An Initial Assessment

Morgan James Bennet[1], Daniel G Kingston[1], and Nicolas J. Cullen[2]

[1]University of Otago
[2]School of Geography

January 3, 2023

## Abstract

Attention is increasingly being turned towards an investigation of extreme hydrometeorological events within the context of land-atmosphere coupling in the wider hydrological cycle, particularly with respect to the identification of compound and seesaw events. To examine these events, accurate soil moisture data are essential. Here, soil moisture from three reanalysis products (ERA5-Land, BARRA and ERA5) are compared to station observations from 12 sites across New Zealand for an average timespan of 18 years. Soil moisture data from all three reanalyses were subsequently used to investigate land-atmosphere coupling with gridded (observational) precipitation and temperature. Finally, compound (co-occurrence of hot and dry) and seesaw (transitions from dry to wet) periods were identified and examined. No best performing reanalysis dataset for soil moisture is evident (min r = 0.78, max r = 0.80). All datasets successfully capture the seasonal and residual component of soil moisture, but not the observed soil moisture trends at each location. Strong coupling between soil moisture and temperature occurs across the predominately energy-limited regions of the lower North Island and entire South Island. Consequently, these regions reveal a high frequency of compound period occurrence and potential shifts in land states to a water limited phase during compound months. A series of seesaw events are also detected for the first time in New Zealand (terminating an average of 17% of droughts), with particularly high frequency of seesaw event occurrence detected in previously identified areas of atmospheric river (AR) activity, indicating the likely wider significance of ARs for drought termination.

## Hosted file

951696_0_art_file_10520014_rmlcdt.docx available at https://authorea.com/users/565239/articles/612255-extreme-compound-and-seesaw-hydrometeorological-events-in-new-zealand-an-initial-assessment

## Hosted file

951696_0_supp_10520015_rmlczt.docx available at https://authorea.com/users/565239/articles/612255-extreme-compound-and-seesaw-hydrometeorological-events-in-new-zealand-an-initial-assessment

# Extreme Compound and Seesaw Hydrometeorological Events in New Zealand: An Initial Assessment

M.J. Bennet[1], D.G. Kingston[1] and N.J. Cullen[1]

[1] *School of Geography, University of Otago, Dunedin, New Zealand*

Corresponding author: Morgan Bennet (morgan.bennet@postgrad.otago.ac.nz)

**Key Points:**

- Reanalysis soil moisture captures seasonal and residual components of observed soil moisture
- Compound events highlight potential changing in land states in wet, energy limited climates
- Seesaw events (one month accumulation) terminate an average of 17% of droughts

**ABSTRACT**

Attention is increasingly being turned towards an investigation of extreme hydrometeorological events within the context of land-atmosphere coupling in the wider hydrological cycle, particularly with respect to the identification of compound and seesaw events. To examine these events, accurate soil moisture data are essential. Here, soil moisture from three reanalysis products (ERA5-Land, BARRA and ERA5) are compared to station observations from 12 sites across New Zealand for an average timespan of 18 years. Soil moisture data from all three reanalyses were subsequently used to investigate land-atmosphere coupling with gridded (observational) precipitation and temperature. Finally, compound (co-occurrence of hot and dry) and seesaw (transitions from dry to wet) periods were identified and examined. No best performing reanalysis dataset for soil moisture is evident (min r = 0.78, max r = 0.80). All datasets successfully capture the seasonal and residual component of soil moisture, but not the observed soil moisture trends at each location. Strong coupling between soil moisture and temperature occurs across the predominately energy-limited regions of the lower North Island and entire South Island. Consequently, these regions reveal a high frequency of compound period occurrence and potential shifts in land states to a water limited phase during compound months. A series of seesaw events are also detected for the first time in New Zealand (terminating an average of 17% of droughts), with particularly high frequency of seesaw event occurrence detected in previously identified areas of atmospheric river (AR) activity, indicating the likely wider significance of ARs for drought termination.

KEYWORDS: Land-Atmosphere, Coupling, Compound Event, Seesaw Event, New Zealand

**Plain Language Summary**

Extreme hydrometeorological events are very damaging, with two examples being compound and seesaw events. Compound events include examples such as droughts and heat waves which occur at the same time, while seesaw events represent shifts from dry (drought) periods to wet (flood) periods. Understanding how these events start, operate and stop can therefore be extremely helpful to help us prepare for them, and reduce their effects. Soil moisture is an essential variable to examine when trying to improve our understanding of these events, as it can help us to understand the interactions between the land (soil) and atmosphere (precipitation and temperature) which occur. Therefore, having accurate soil moisture data is an important goal. This study investigates how well soil moisture is represented across New Zealand from three products, revealing all products to be similar in their performance. The study then investigates the land-atmosphere interactions across New Zealand, revealing widespread declines in soil moisture during the summers between 1990 and 2018. Compound events show a high occurrence in traditionally wet environments, indicating changes in the land state during drought phases. Rapid transitions from dry to wet are revealed in areas previously identified as being exposed to extreme rainfall.

## 1. Introduction

Extreme hydrometeorological events can be very damaging. For instance, summer heatwaves throughout Europe during 2018 caused many fatalities, including an estimated 2363 across France and the United Kingdom (Moravec *et al*., 2021), while the 2017-2019 multiyear drought across New South Wales in Australia was estimated to have had an economic impact of $53 billion (Wittwer and Waschil, 2021). Correspondingly, improved characterisation of the drivers of these events (including climate change) is a critical research goal. While research on uni variate extreme hydrometeorological events is widespread (e.g. Donat *et al.*, 2016; Perkins-Kirkpatrick and Lewis, 2020; Spinoni *et al.*, 2020), increasingly attention is being turned towards a more holistic investigation of extreme hydrometeorological events, examining them as part of the wider hydrological cycle to which they belong (Dirmeyer *et al.*, 2021). Two examples of these are compound (Zscheischler *et al.*, 2020) and seesaw (or whiplash) (Ficklin *et al.*, 2022) events.

Compound events represent the co-occurrence of multiple dependent hazards whose effects may be greater than the sum of their parts. (Zscheischler *et al*., 2018). For example, Manning *et al*. (2019) identified an increased probability of compounding dry and hot events throughout Europe, driven by rising temperatures in the region. In contrast, seesaw events represent dramatic swings from drought (dry) to pluvial (wet) conditions. This rapid hydrometeorological switch can pose substantial risk to water management practices (e.g. the Oroville Dam crisis in California (Wang *et al*., 2017)). The turn in focus to examining the hydrological cycle collectively is required to understand the complex interactions which drive these events i.e. the role of soil moisture during the development of hot and dry compound events (Dirmeyer *et al.*, 2021) or as a measure of propagation of drought termination through the hydrological cycle during seesaw events (He and Sheffield, 2020).

In exploring this more holistic approach to extreme hydrometeorological events, the role of soil moisture emerges as a key component due to the feedback loops present in the interaction between land and atmosphere (Seneviratne *et al.*, 2010), requiring data which accurately portrays this process. Similarly, an important first step in investigating extreme hydrometeorological events is to first gain a broader understanding of the land-atmosphere interactions (i.e. coupling) and dependence structure between hydrometeorological variables (e.g. soil moisture and temperature / precipitation) across the study area (Tootoonchi *et al.*, 2022). In doing so, a more refined focus is able to be developed to target specific event types i.e. compounding and seesaw behaviour.

Representation of soil moisture on large spatial scales is often performed via satellite imaging, which are typically on a coarse resolution (Gruber *et al.*, 2020), and as such lack the fine resolution required for heterogeneous landscapes such as those found in New Zealand. With the improved spatial resolution offered by current generation reanalysis products, the representation of soil moisture within these models is of key interest (Gevaert *et al.*, 2018). Greater accuracy in soil moisture representation has been highlighted in the current generation reanalysis datasets across large spatial scales (Ling *et al*., 2021; Muñoz-Sabater *et al*., 2021). However, Li *et al*. (2020) identified a need for more regional performance assessments involving fine scales and diverse topography. New Zealand, displaying a complex topography and varied climate (Macara, 2018), is an ideal candidate for such an assessment.

The primary and most commonly employed dataset for soil moisture analysis in New Zealand involves a simple water balance approach (Porteous *et al.*, 1994) driven by a high-resolution precipitation and potential evapotranspiration (PET) dataset based on statistical interpolation of station observations (the Virtual Climate Station Network (VCSN; Tait *et al.*, 2012; Tait and Woods, 2007)). Such an approach, while computationally simple and available on a fine resolution, cannot accurately mimic the soil-vegetation-atmosphere coupling represented in climate model simulations of the terrestrial water cycle (Berg and Sheffield, 2018). For example, PET becomes increasingly misrepresentative of actual evapotranspiration (AET) under a warming atmosphere due to the physiological effects of $CO_2$ on plant water needs (Swann *et al*., 2016). As a result, Berg and Sheffield (2018) recommended the use of model outputs rather than offline proxy metrics for analysis of soil moisture. Therefore, despite the apparent greater accuracy in the representation of driving variables for soil moisture within the VCSN dataset (Tait *et al.*, 2012; Tait and Woods, 2007), the resultant soil moisture dataset may be inappropriate for examination of extreme hydrometeorological events across the country, particularly under a changing climate (Berg and Sheffield, 2018).

With new evidence highlighting agreeable performance in the most recent generation of reanalysis datasets in the presentation of precipitation and temperature (Pirooz *et al.*, 2021), accurate representation of soil moisture within the same datasets may allow for a focused examination on the land-atmosphere coupling in locations such as New Zealand. As noted by Dirmeyer *et al.* (2021), land-atmosphere coupling has been shown to exacerbate both heat waves and droughts via widespread soil water declines and subsequent dominance of sensible heat in surface flux partitioning in similar climates to New Zealand. Understanding the role this land-atmosphere coupling has on the severity of high temperature extremes is therefore critical within the context of a warming climate, while focusing research on the role land-atmosphere coupling plays during extreme hydrometeorological events could provide new key findings on both heat waves and drought. Similarly, the rapid transition of land states from dry to wet (or vice versa) is governed by hydrological persistence, itself controlled by land-atmosphere coupling via the partitioning of surface fluxes (Ferguson and Wood, 2011; He and Sheffield, 2020). Thus, an examination of land-atmosphere coupling may also provide insight into these damaging oscillations in hydrological states by revealing key drivers during the transitional phase.

For New Zealand, the role of land-atmosphere coupling is poorly understood, with no country-wide study yet performed, despite continued research into drought, heat wave and extreme precipitation events across the country (e.g. Bennet and Kingston, 2022; Reid *et al*., 2021; Salinger *et al*., 2019). For example, Salinger *et al*. (2019) identified high temperatures across New Zealand during the 2017/2018 summer which were coupled to sea surface temperatures. However, the role that land-atmosphere coupling played in either exacerbating the high temperatures or which resulted in rapid surface drying remains unexplored. With New Zealand covering multiple climate zones, understanding the characteristics and variation of extreme hydrometeorological events across this mosaic of climates is vital.

Here, land-atmosphere coupling is investigated using soil moisture as a proxy, given the controlling nature of soil moisture and its role as a critical variable in land-atmosphere exchanges, with the strength of coupling defined by the correlation between soil moisture (land) and precipitation / temperature (atmosphere). The primary aim of this study is to examine the land-atmosphere coupling across New Zealand, and its role during compound and seesaw events. In doing so, the role of soil moisture and land-atmosphere coupling during these compound and seesaw events would, for the first time, be able to be explored in a New Zealand context. Within this primary aim, the relative performance of soil moisture simulation in the current generation reanalysis products will be compared, including an examination of the skill in replicating observed soil moisture within these reanalysis products.

The findings will thus provide new insight into land-atmosphere coupling for New Zealand, as well as provide a first look at compound and seesaw events for the country. With the wide climatological diversity across New Zealand, the findings will be informative more widely, particularly those concerned with the representation of these interactions at a fine resolution. The relative performance of reanalysis datasets in representing these interactions, and on the representation of soil moisture across the varied climate and topography, is expected to also be informative for the ongoing development of reanalysis products both locally, regionally and internationally.

## 2. Data and Methods

### 2.1. Datasets

#### *2.1.1. Reanalysis Datasets*

Hourly soil moisture data were obtained from the European Reanalysis 5$^{th}$ Generation (ERA5; Hersbach *et al*., 2020), European Reanalysis 5$^{th}$ Generation Land Component (ERA5-Land; Muñoz-Sabater *et al*., 2021) and the Bureau of Meteorology (BOM) Atmospheric High-resolution Regional Reanalysis for Australia (BARRA-R; Su *et al*., 2019), for the period 1 January 1990 to 31 December 2018. Hourly data were first aggregated into daily and then monthly means, before conversion to mm of water.

ERA5 is available at a 0.25°x0.25° resolution at hourly intervals (Hersbach *et al*., 2020), while ERA5-Land available at a resolution of 0.1°x0.1° and at an hourly temporal resolution (Table 1). In contrast to ERA5 and ERA5-Land , BARRA assimilates additional land-surface observations for New Zealand from the National Climate Database (CliFlo; NIWA, 2021), with the resulting model output from BARRA performing better for precipitation and temperature than both ERA5-Land and ERA5 (Pirooz *et al*., 2021). BARRA is available on a 0.12°x0.12° resolution at 10 minute to hourly intervals (Su *et al*., 2019).

**Table 1.** Information on reanalysis and gridded climate products used in the study

| Dataset | Description | Period Available | Spatial Resolution (Horizontal) | Land Model | Soil Layer Depths (cm) | Coordinates (lat (min, max) / lon (min, max)) | Reference |
|---|---|---|---|---|---|---|---|
| VCSN | Gridded, interpolate station observations | 1 Jan 1972 – Present | 0.05°x0.05° | NA (Interpolated) | Unknown | 166.475, 178.475 / -47.275, -34.425 | Tait and Turner (2005) |
| ERA5-Land | HTESSEL driven by downscaled ERA5 | 1 Jan 1950 – Present | 0.10°x0.10° | HTESSEL | 7, 28, 100, 289 | 166.30, 178.70 / -47.50, -34.30 | Muñoz-Sabater *et al*. (2021) |
| BARRA | UM, initiated by ERA-Interim | 1 Jan 1990 – 28 Feb 2019 | 0.12°x0.12° | JULES | 10, 35, 100, 300 | 166.42, 178.63 / -47.29, -34.42 | Su *et al*. (2019) |
| ERA5 | IFS Cycle 41r2 | 1 Jan 1979 - Present | 0.25°x0.25° | HTESSEL | 7, 28, 100, 289 | 166.50, 178.75 / -47.25, -34.25 | Hersbach *et al*. (2020) |

### *2.1.2. Soil Moisture Standardisation*

A graphical illustration of the methodological framework employed in the present study is contained in Fig. S2. To describe: ERA5-Land and ERA5 both contain soil moisture at four depths (0-7, 7-28, 28-100 and 100-289 cm), while the BARRA dataset similarly contains soil moisture at four different depths (0-10, 10-35, 35-100 and 100-300 cm). For comparative purposes, only the first two depths were accessed for each dataset, as observations (Section 2.1.4) are taken at a 20 cm profile depth. For the BARRA dataset, conversion to fractional volumetric soil moisture ($m^3\,m^{-3}$) was first required before applying the procedure of Li *et al*. (2005) (Equations 1 and 2). Equation 1 denotes the procedure for ERA5-Land and ERA5, while Equation 2 denotes the procedure for BARRA.

$$W = 200(0.35 \times \theta_1 + 0.65 \times \theta_2) \quad (1)$$

$$W = 200(0.5 \times (\theta_{v1}/100) + 0.5 \times (\theta_{v2}/250)) \quad (2)$$

where W represents the soil moisture (mm) in the top 20 cm of soil, $\theta_1$ represents the volumetric soil moisture for layer one (0-7 cm, ERA5-Land and ERA5; 0-10 cm, BARRA) and $\theta_2$ the volumetric soil moisture for layer two (7-28 cm, ERA5-Land and ERA5; 10-35 cm, BARRA) (adapted from Li *et al*. (2005)).

### *2.1.3. Precipitation and Temperature Gridded Datasets*

The Virtual Climate Station Network (VCSN), complied and hosted by the National Institute of Water and Atmospheric Research (NIWA), was selected to provide precipitation and temperature data. VCSN provides daily estimates of climatic data on a 5km grid covering New Zealand (Tait and Turner, 2005).

VCSN data were accessed for 1 January 1990 to 31 December 2018. Daily estimates are produced based on the daily interpolation of actual data observations made at climate stations located across the country (Tait and Turner, 2005). Temperature was available as daily minimum and maximum values. Monthly means of both minimum and maximum temperature were first calculated, before monthly mean temperature was obtained as the average of the monthly minimum and maximum temperature. Daily precipitation data were summed across each month.

Due to the different grid cell resolutions of the reanalysis products, VCSN monthly total precipitation and mean temperature were regridded (aggregated) to the native resolution of each reanalysis dataset (Table 1.1). Aggregation was performed using the nearest neighbour method. As analysis was performed on a monthly time step, the ability to capture the statistical properties at fine resolutions was not a dominating consideration (Rajulapati *et al*., 2021).

### *2.1.4. Station Observations*

To enable comparisons against specific locations, ground station observations of soil moisture were obtained from the NIWA Automatic Weather Station (AWS) network (CliFlo climate database; NIWA, 2021). Mean monthly soil moisture was used. Soil moisture measurements taken at all locations are at a standard depth of 20 cm (NIWA, 2021).

Twelve locations were selected as ground station observations (Fig. 1), to best represent the complex and varied climate across New Zealand. Locations were first selected based on the seven station temperature series (7SS) of Mullan *et al*. (2010), originally designed to sample from most parts of New Zealand and which is often used as basis for understanding the national temperature response to climate change. Reefton replaced the Hokitika 7SS location, Paraparaumu replaced Wellington, Martinborough replaced Masterton and Hamilton replaced Auckland, all due to the lack of consistent soil moisture data at the original locations. Additional stations have been added to capture greater variety of climatic regions throughout New Zealand (Kaitāia, Gisborne, Stratford, Invercargill and Lauder) (Fig. 1). The longest station record was Kaitāia (November

1999), with the shortest at Hamilton (December 2005), with an average length of record across all 12 sites of 18 years / 212 months (n = 2539) (Table S1).

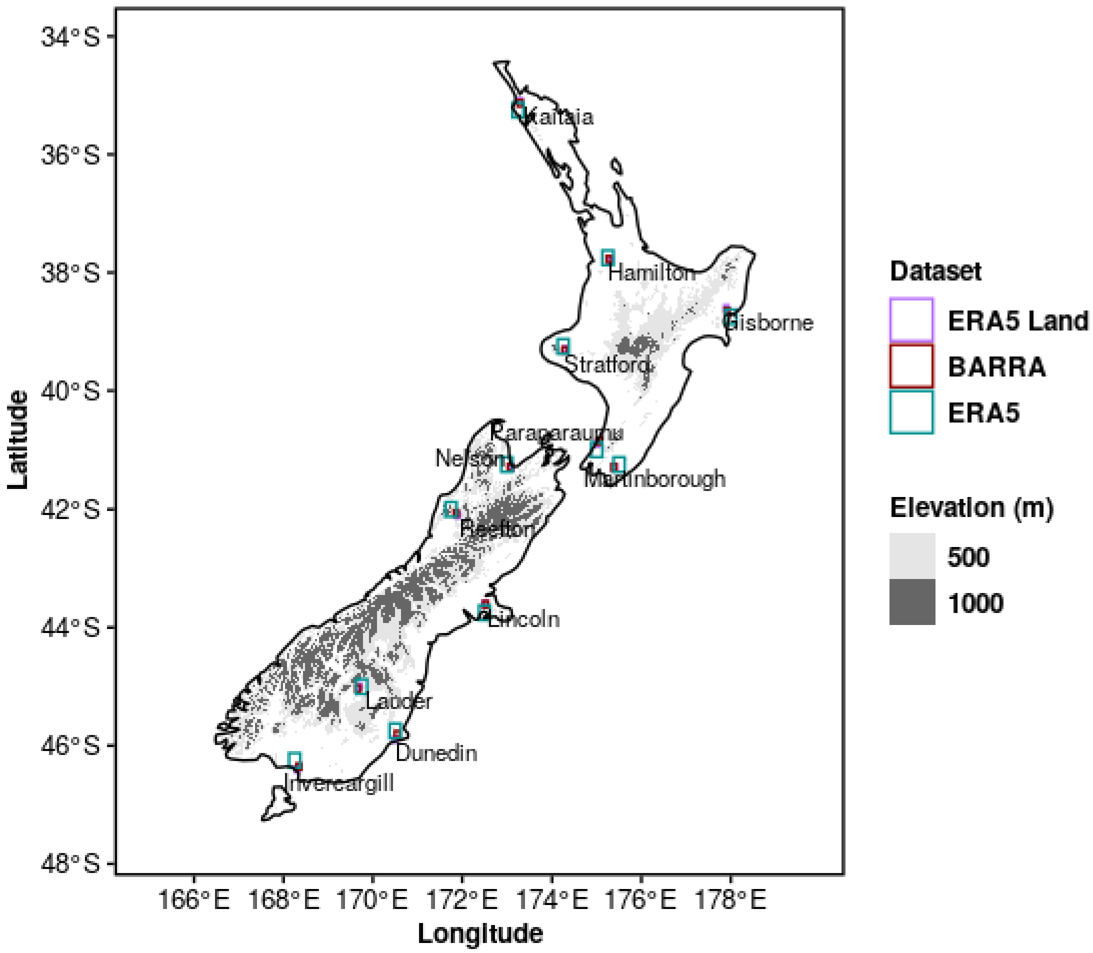


**Fig. 1** Observational site locations and grid cell locations from each reanalysis dataset (boundaries as represented by colouration) used for statistical analysis. Elevation is represented by grey scale.

A missing monthly value is outputted from CliFlo if there are more than 10 (or 5 consecutive) missing daily observations within a selected month, which numbered n = 34 (1.34%) in the current work. For missing values, the average monthly value for the month concerned was taken across the entire time series of that selected station (i.e. a mean of all January's for the relevant station across the entire time series). The CliFlo database returns soil moisture as a percentage of the total soil volume (soil profile depth of 20 cm), with conversion to mm of water being performed by multiplying the percentage of total soil volume by the soil profile depth.

## 2.2. Analysis of Soil Moisture Observations to Reanalysis Datasets

The closest grid cell at each observation location was identified from each reanalysis dataset (Fig. 1). Subsequent analysis was then performed between these ground station measurements and grid cell values, with the time series length stipulated by the length of the station record (Table S1).

Annual cycles at each location were calculated as the mean of each month for all datasets (observations, ERA5-Land, BARRA and ERA5), thereby creating a 12 station series of soil moisture for New Zealand. A single time series for each dataset was also constructed by integrating the data across all 12 locations (i.e. mean of all locations; 12 stations), with standard deviations also shown. These dataset mean time series were then further analysed by performing seasonal trend decomposition, to reveal the underlying trend, seasonal and residual components of the original time series. Seasonal trend decomposition was performed using the Seasonal and Trend decomposition using Loess method (STL; Cleveland *et al*., 1990), following the best practice recommended by Gruber *et al*. (2020). These underlying components were analysed using Root Mean Square Error (RMSE) and correlation (Pearson's r; Pearson, 1895), with the trend component further analysed by applying ordinary least square regression on each dataset.

At each location, a range of statistical analyses were conducted. Pearson's correlation coefficients were calculated between the observational data and the corresponding reanalysis grid cells. Pearson correlation coefficient was used as a measure of temporal variability, with its use insensitive to the inherent scale discrepancy between comparing in situ measurements and model grid cells (Gruber *et al*., 2020). Standard deviation was calculated within each dataset at each location, while the trend in the data at each site (as expressed by each 11atasett) was calculated as the linear trend using ordinary least square.

## 2.3. Soil Moisture and Precipitation / Temperature Coupling

The representation of land-atmosphere coupling across New Zealand was also investigated, via a simple correlation (Kendall's $\tau$; Kendall, 1938) between monthly mean soil moisture and total precipitation/mean temperature. While correlation cannot demonstrate causality, it can provide an indication of possible physical relationships, especially where causality has already been established (Seneviratne *et al*., 2010), and has been used successfully to evaluate land-atmosphere coupling (Knist *et al*., 2017, Li *et al*., 2017). Monthly total precipitation and mean temperature data from the VCSN (Tait and Turner 2005) were aggregated to the native resolution of each individual reanalysis soil moisture dataset (ERA5-Land, BARRA and ERA5). The VCSN dataset was selected to set a consistent representation of precipitation and temperature, allowing any differences in land-atmosphere coupling to then be attributed to the representation of soil moisture within each dataset.

Insightful understanding of land-atmosphere coupling can be gained from investigating across spatial and temporal lengths wider than those allowed by observation data (Gentine *et al*., 2019). The removal of observational data from this part of the analysis allowed the study period to be extended back to the length of the shortest reanalysis dataset (1990 – BARRA; see Table 1). These extended time series were again decomposed to exclude the seasonal component using STL (Cleveland *et al*., 1990), before restricting the datasets to the growing season, herein defined as November – March (Salinger, 1987). The focus on growing season was made because of the stronger land-atmosphere coupling typically experienced during the period (Chen and Dirmeyer, 2020). Seasonality was removed to enable more rigorous evaluation of the coupling in mean soil moisture and total precipitation / mean temperature (Li *et al*., 2020), on the knowledge that seasonal cycles are well captured in reanalysis products (Jiao *et al*., 2021).

Trends in total precipitation and mean temperature were calculated at the grid cell level in the deseasoned, growing season time series from 1990-2018, using least square regression. Trends were also calculated for mean soil moisture from each reanalysis dataset. Deseasoned mean soil moisture for the growing seasons from 1990 to 2018 from each of the reanalysis datasets was compared to the aggregated, deseasoned total precipitation and mean temperature for the growing seasons from 1990 to 2018, using the Kendall's $\tau$ correlation metric.

The aggregated, deseasoned total precipitation, mean temperature and mean soil moisture (from each reanalysis product), was interrogated for the entire time period; January 1990 to December 2018 (i.e. no growing season restriction). The data were first filtered into dry and wet periods, representing the lowest/highest third of monthly mean soil moisture (n = 116). Monthly soil moisture from each dataset were first ranked from highest to lowest, before selecting the top and bottom third to represent the wet and dry periods. Total precipitation and mean temperature were then also restricted to these same monthly dates and coupling strength (Soil Moisture-Precipitation (SM-P); Soil Moisture-Temperature (SM-T)) then calculated using Kendall's $\tau$.

### 2.4. Compound and Seesaw Events

Accurate representation of soil moisture is equally important for the study of individual extreme hydrometeorological events (Fischer *et al*., 2007; Sheffield *et al*., 2004; Sivapalan *et al*., 2005), and when investigating compound and seesaw event behaviour (He and Sheffield 2020; Whan *et al*., 2015). Here, the raw monthly total precipitation and monthly maximum temperature, for each aggregated VCSN dataset, was first standardised to a normal distribution, with a mean of zero and standard deviation of one. A one-month accumulation period was utilised, while 12 distributions were fitted (i.e. one for each month) to account for seasonal differences (Kao and Govindaraju, 2010). Standardisation was achieved via the Gamma distribution (precipitation; Standardised Precipitation Index, SPI) (McKee *et al*., 1993), the normal distribution (temperature; Standardised Temperature Index, STI) (Zscheischler *et al*., 2014), and the Beta distribution (Standardised Soil Moisture Index; SSMI) (Hao and AghaKouchak, 2014; Sheffield *et al*. 2004).

After transformation to the standard normal distribution, compound events were defined as the co-occurrence of soil moisture (SSMI) below -1, and maximum temperature (STI) above 1 (i.e. bottom/top 32%) at each grid cell to describe the joint dry (soil moisture) and hot (temperature) conditions. This co-occurrence of extremes was examined both as counts of the number of occurrences (months) across the time series (1990-2018), and by applying a Mann-Kendall test (Mann, 1945) at each grid cell to identify any trend in the co-occurrences of hot and dry conditions (Feng *et al*., 2021). This process was repeated for each reanalysis dataset.

Seesaw events were defined and examined using the procedure of He and Sheffield (2020): an Event Coincidence Analysis (ECA) (Siegmund *et al*., 2017) was undertaken to identify how frequently droughts (dry periods) are followed by pluvials (wet periods), with a mutual delay of 1 month to capture rapid transitions in hydrometeorological states. The use of a 1 month delay differs to that of He and Sheffield (2020) who employed a 3 month delay to capture seasonal scale transitions. In simple terms, the 1 month delay reflects a change from drought conditions to pluvial conditions during the following month, thus capturing abrupt endings to dry phases. Poisson based significance tests were also applied to each land grid cell to identify if the estimated seesaw event occurrence was significant or not. Further in-depth details of the process are contained in the work of He and Sheffield (2020) and Siegmund *et al*. (2017). For seesaw events, droughts were defined as any month below the -1 threshold in the SSMI dataset, with pluvials identified as those months above the +1 threshold in the SPI. The occurrence of both droughts and pluvials, defined by exceedance of precipitation at the -1/1 level (SPI) was also performed. This process was again repeated for each reanalysis dataset.

## 3. Results

### 3.1. Soil Moisture Comparison

Observational data shows a clear seasonal cycle at all sites (Fig. 2). Peaks in soil moisture occur in late winter (July/August), with the lowest values recorded in late summer or early autumn (February/March). The highest average soil moisture is recorded at Nelson (123 mm), while the lowest average soil moisture is recorded at Paraparaumu (17 mm). Annual cycles at each site show varying degrees of performance across the reanalysis datasets, with no one dataset emerging as better performing (median correlation of 0.79). Martinborough (ERA5-Land; range of 1 mm and BARRA; range of 4 mm) and Stratford (ERA5; range of 5 mm) show the smallest deviation in annual cycles to observations, while Nelson shows the largest (all reanalysis datasets; average range of 48 mm).

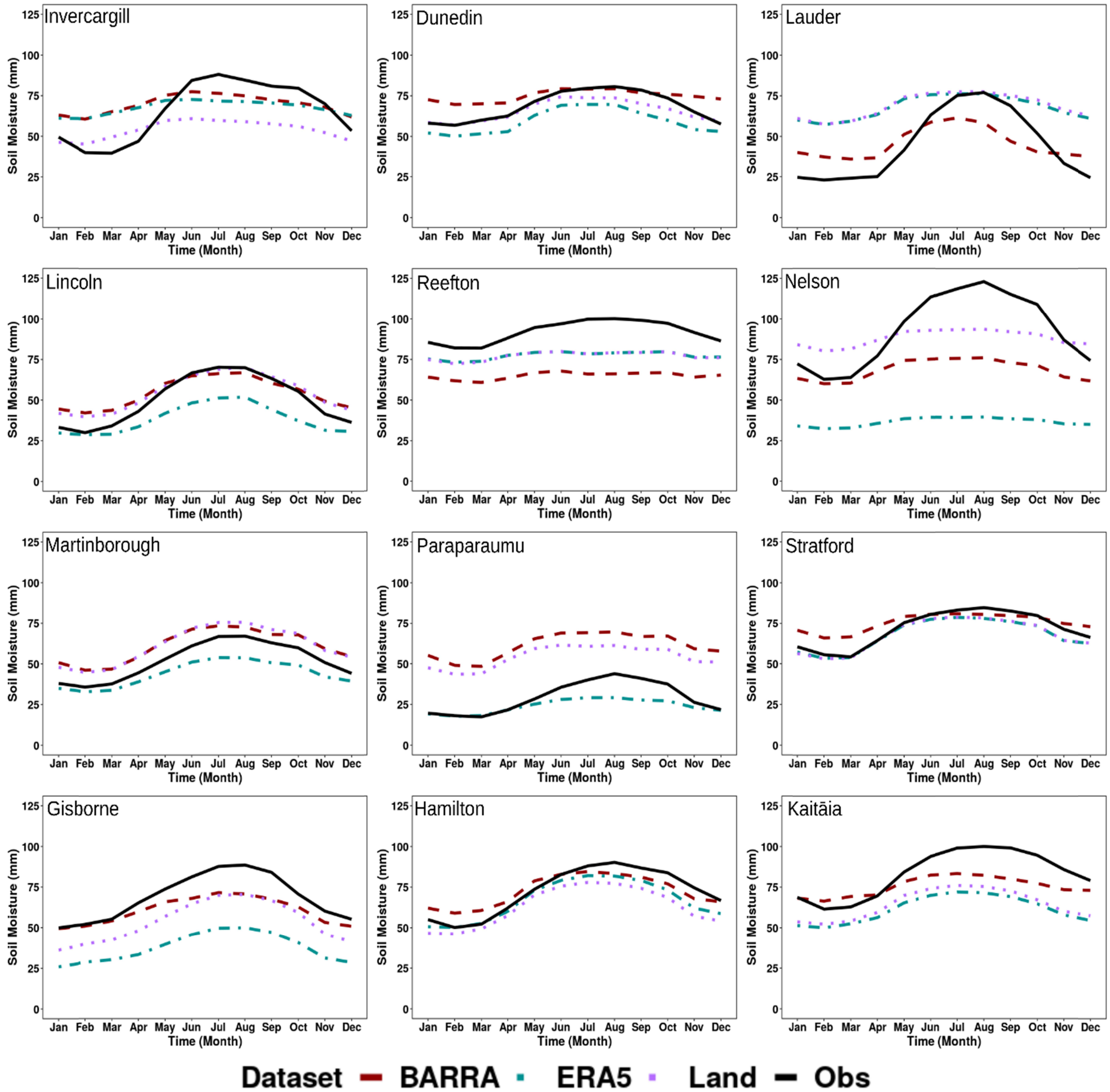


**Fig. 2** Annual cycles of site-averaged monthly mean soil moisture over the 12 observational locations and corresponding reanalysis datasets, for a range of time periods (1999-2018; see Table S1).

Integrated time series (mean of all 12 locations) highlights moderate to strong correlations between the decomposed time series components of observations and reanalysis datasets (Fig. 3; correlations of 0.67 to 0.99). Stronger variation is present in the observations, with ERA5-Land best able to capture this variation (Table 2; standard deviation 8.96). ERA5-Land shows the greatest agreement in magnitude terms (smallest RMSE, 14.01), with ERA5 revealing a consistent smaller magnitude than observational data. Observational data reveals a statistically significant increasing trend in soil moisture (0.57 mm $yr^{-1}$). No reanalysis dataset is able to capture the statistically significant increasing trend seen in the observations. Correlation in the trend components (after STL decomposition) is strongest with observations and ERA5 (0.80), while weakest with ERA5-Land (0.67), while RMSE is largest between ERA5 and observations (18.22), and smallest with BARRA (6.80).

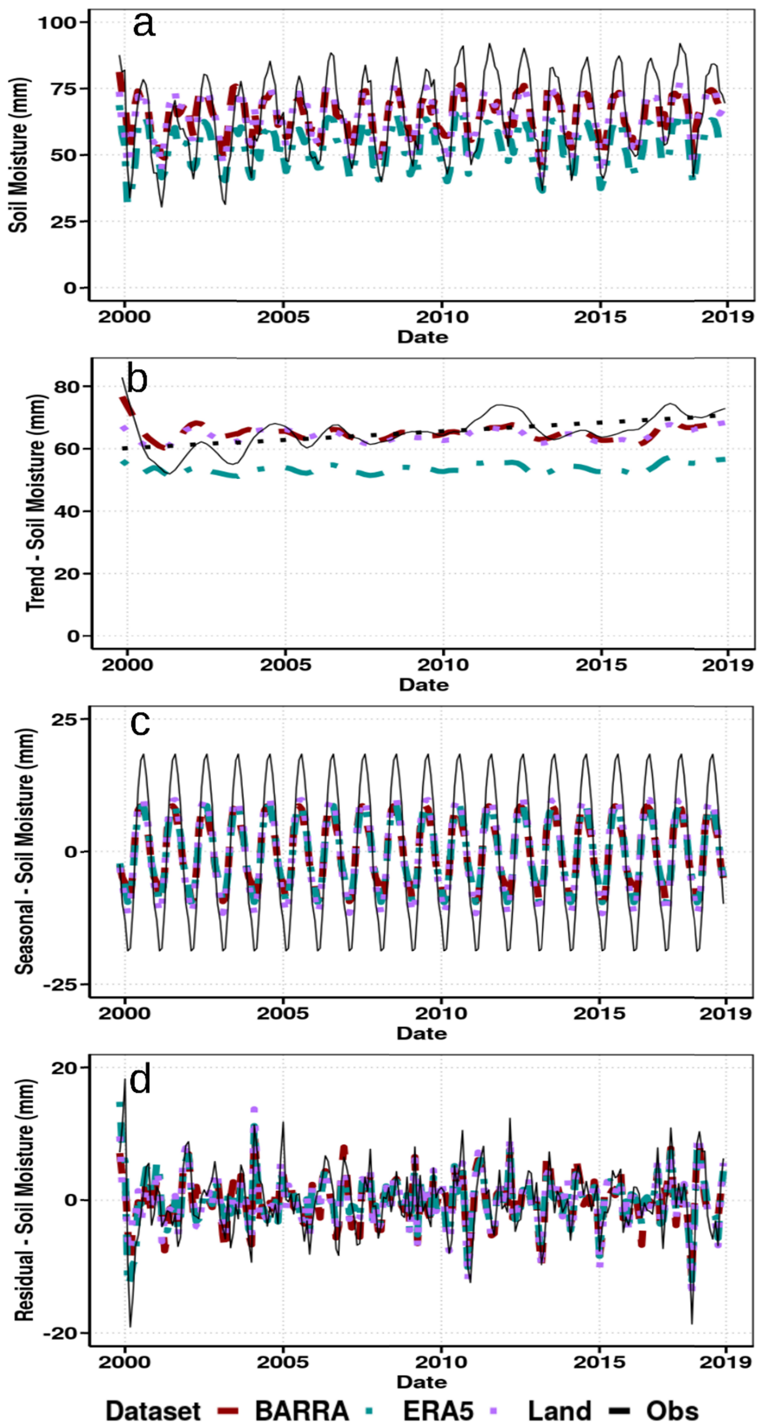


**Fig. 3** Time series decomposition (STL) of monthly mean soil moisture integrated across all 12 sites (observations and associated grid cells for reanalysis datasets; for a range of time periods (1999-2018; see Table S1)). Showing (a) original time series, (b) trend component, (c) seasonal component and (d) residual component. Note the different axis range in each panel. The blacked dotted line in panel (b) signifies the linear trend in observational data, significant at the 1% level.

**Table 2.** Statistics of seasonal trend decomposition (performed using STL) of the reanalysis datasets soil moisture and observational soil moisture (see Figure 3).

| Statistic | Category | ERA5 Land | BARRA | ERA5 |
|---|---|---|---|---|
| Standard Deviation (15.35 for Obs) | | 8.96 | 7.73 | 7.64 |
| Correlation Coefficients | Time Series | 0.91 | 0.89 | 0.92 |
| (Reanalysis and Observations) | Trends | 0.67 | 0.68 | 0.80 |
| | Seasonal | 0.98 | 0.97 | 0.99 |
| | Residual | 0.79 | 0.78 | 0.84 |
| Root Mean Square Error | Time Series | 14.01 | 16.62 | 19.35 |
| (Reanalysis and Observations) | Trends | 6.97 | 6.80 | 18.22 |
| | Seasonal | 58.98 | 63.53 | 50.98 |
| | Residual | 1309.20 | 1721.50 | 1423.83 |
| Linear Trend (0.56 mm $yr^{-1}$ for Obs) | | 0.09 | 0.02 | 0.12 |

Correlations between the seasonal component of the integrated time series demonstrates ERA5 as the best performing (0.99), followed by ERA5-Land (0.98) and then BARRA (0.97) (Fig. 3; Table 2). ERA5, ERA5-Land and then BARRA show decreasing ability in capturing the residual range, although a smaller RMSE is present between the residuals of ERA5-Land and the observations (1309.20). All reanalysis datasets capture anomalous conditions present in the observational dataset, such as the summers of 1999/2000 and 2017/2018.

All reanalysis datasets show a frequent underestimation of high values and overestimation of low values when compared to observations (Fig. 4). The smallest mean differences between reanalysis datasets and observations are found at Dunedin (ERA5-Land; 3 mm), Hamilton (BARRA; 1 mm) and Invercargill (ERA5; 2 mm), while the largest occur at Paraparaumu (ERA5-Land; 25 mm and BARRA; 32 mm) and Nelson (ERA5; 57 mm). Paraparaumu reveals a consistent overestimation in ERA5-Land and BARRA, while only ERA5 shows this overestimation at low values. A consistent underestimation of observational data by ERA5 is found at Nelson and Gisborne. Similar distributions are seen across all three reanalysis datasets at Stratford, with Hamilton revealing the largest differences in the representing of soil moisture to observations across all three reanalysis datasets.

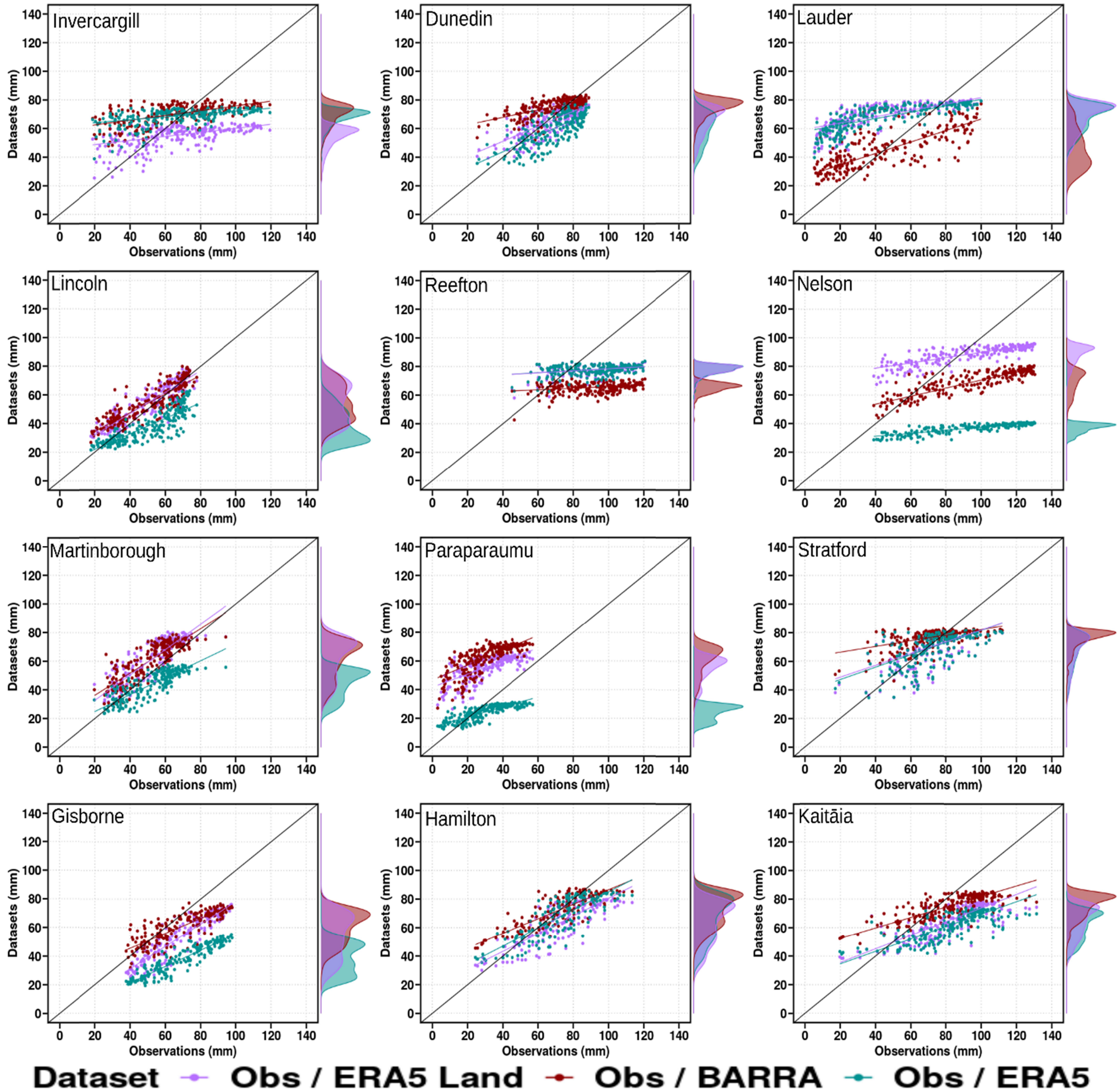


**Fig. 4** Scatterplots between observational data and reanalysis datasets (monthly mean soil moisture) at each location, including marginal distributions of each dataset. The solid black line denotes a 1:1 line.

There is no clear best performing reanalysis dataset when assessed on the correlation of the entire time series at each station (Table 3), although median correlation is slightly higher for ERA5 (0.80). Gisborne has the strongest average correlation across the datasets (0.88), while Reefton has the lowest (0.37). Martinborough, Stratford, Hamilton and Kaitāia are all in close agreement in correlation coefficients, while Gisborne has the largest difference (range of 0.11). Reanalysis datasets show similar standard deviations at all sites, with similar median scores (range of 0.88). The largest difference in standard deviations between observations and datasets occurs at Nelson (ERA5; 23.44), while ERA5-Land shows the smallest difference to observational standard deviation at Martinborough (0.08).

**Table 3.** Summary statistics of soil moisture (correlation, standard deviation and trend) at each location, between observations and the corresponding grid cell from each reanalysis dataset. Statistical significance (p=0.05) is indicated by yellow highlighting.

| Statistics | Location | Observations | ERA5 Land | BARRA | ERA5 |
|---|---|---|---|---|---|
| Correlation | Invercargill | - | 0.60 | 0.60 | 0.57 |
| | Dunedin | - | 0.77 | 0.68 | 0.75 |
| | Lauder | - | 0.75 | 0.74 | 0.78 |
| | Lincoln | - | 0.91 | 0.86 | 0.85 |
| | Reefton | - | 0.41 | 0.32 | 0.39 |
| | Nelson | - | 0.82 | 0.86 | 0.85 |
| | Martinborough | - | 0.84 | 0.84 | 0.83 |
| | Paraparaumu | - | 0.73 | 0.76 | 0.83 |
| | Stratford | - | 0.61 | 0.62 | 0.62 |
| | Gisborne | - | 0.92 | 0.81 | 0.92 |
| | Hamilton | - | 0.82 | 0.83 | 0.83 |
| | Kaitāia | - | 0.79 | 0.79 | 0.78 |
| | Median | - | 0.78 | 0.78 | 0.80 |
| Standard Deviation | Invercargill | 24.63 | 7.75 | 7.38 | 6.16 |
| | Dunedin | 13.88 | 9.51 | 6.10 | 10.86 |
| | Lauder | 27.90 | 9.57 | 13.66 | 9.01 |
| | Lincoln | 16.83 | 13.48 | 12.40 | 10.92 |
| | Reefton | 17.10 | 4.03 | 3.74 | 3.72 |
| | Nelson | 26.81 | 6.40 | 8.39 | 3.37 |
| | Martinborough | 14.04 | 13.96 | 12.79 | 9.54 |
| | Paraparaumu | 12.82 | 8.95 | 10.19 | 5.25 |
| | Stratford | 17.06 | 11.87 | 7.05 | 11.56 |
| | Gisborne | 17.16 | 14.76 | 30.72 | 10.37 |
| | Hamilton | 18.64 | 14.17 | 11.13 | 14.24 |
| | Kaitāia | 20.01 | 10.77 | 8.11 | 9.50 |
| | Median | 17.13 | 10.17 | 9.29 | 9.52 |
| Trend (mm $\text{yr}^{-1}$) | Invercargill | 0.97 | -0.02 | 0.02 | -0.04 |
| | Dunedin | 0.79 | 0.17 | 0.12 | 0.19 |
| | Lauder | 1.01 | -0.03 | 0.14 | 0.05 |
| | Lincoln | 0.07 | 0.37 | 0.03 | 0.29 |
| | Reefton | 0.09 | 0.00 | -0.03 | 0.00 |
| | Nelson | 0.52 | 0.10 | 0.03 | 0.05 |
| | Martinborough | -0.57 | 0.27 | 0.03 | 0.27 |
| | Paraparaumu | 0.54 | 0.20 | 0.06 | 0.18 |
| | Stratford | 2.19 | -0.06 | 0.01 | -0.04 |
| | Gisborne | 0.80 | 0.04 | -0.08 | 0.06 |
| | Hamilton | 0.76 | 0.33 | 0.20 | 0.33 |
| | Kaitāia | 0.60 | 0.03 | 0.03 | 0.06 |
| | Median | 0.68 | 0.07 | 0.03 | 0.06 |

All datasets fail to adequately capture the range of trends in observational data at each station (Table 3), with an observed median trend of 0.68 mm yr$^{-1}$ and a median trend range of 0.04 mm yr$^{-1}$ across the three reanalysis datasets. Statistically significant trends are found in observational data at all locations apart from Lincoln, Reefton, Nelson and Hamilton. BARRA does not capture any statistically significant trends. While observational data show no statistically significant trend at Lincoln, both ERA5-Land and ERA5 do. ERA5 records a statistically significant trend at Paraparaumu (albeit weaker than that in the observed data at this site), but registers a significant positive trend at Martinborough when the observations show a significant negative trend. The largest difference in trend occurs at Stratford (ERA5-Land; 2.25 mm yr$^{-1}$), with the smallest difference occur at Lincoln (BARRA; 0.04 mm yr$^{-1}$). Lincoln also has the largest range in trends (0.34 mm yr$^{-1}$) across the reanalysis datasets, with Reefton and Kaitāia having the smallest spread in trend (0.03 mm yr$^{-1}$).

## 3.2. Land-Atmosphere Coupling

Statistically significant declines in precipitation (VCSN; country wide average of -0.61 mm per growing season) are found across the lower North Island, north-west South Island and parts of the Southern Alps, while the highest elevation regions of the Southern Alps show significant increases (Fig. 5). Statistically significant temperature (VCSN) increases occur across most of the country (country wide increase of 0.04 °C per growing season), with the exception of inner montane regions in the middle of the South Island and northeastern areas of both islands.

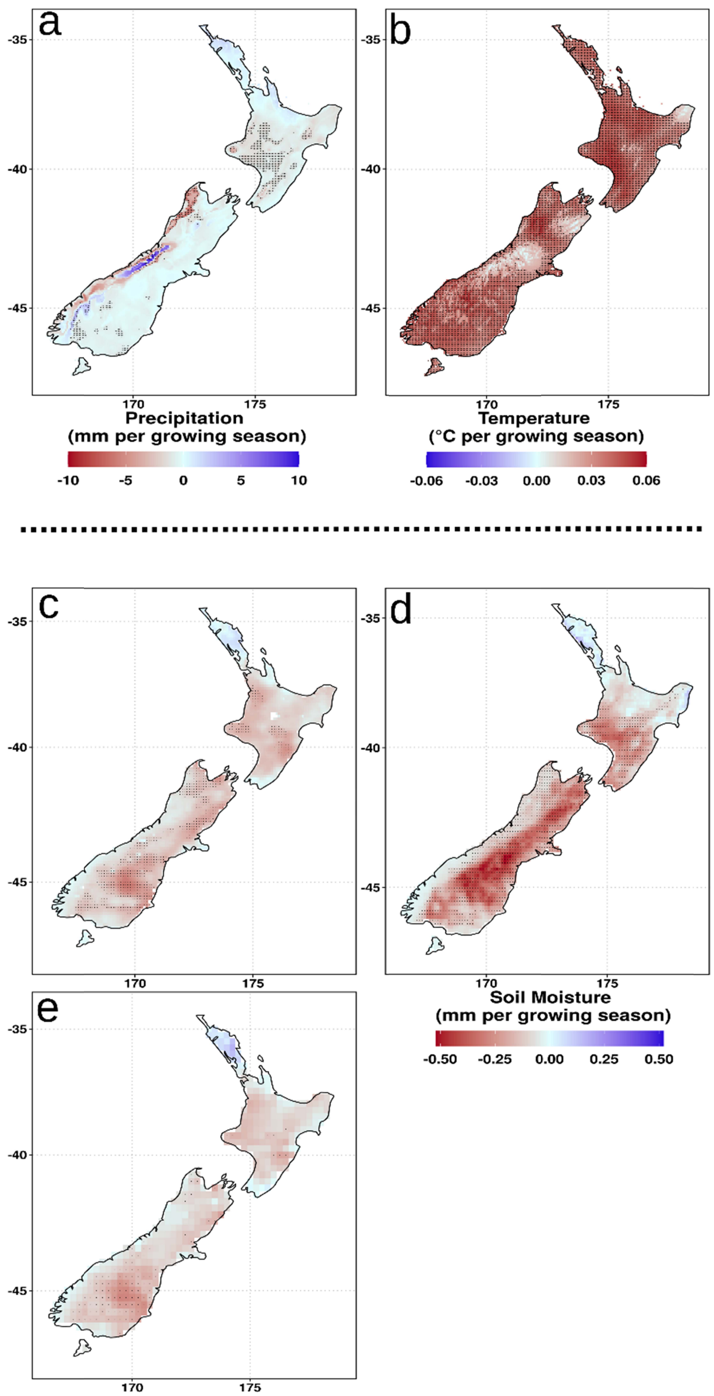


**Fig. 5** Linear trend patterns of monthly total precipitation (a) and mean temperature (b) (VCSN) at individual grid cells over New Zealand during the growing season (Nov-Mar) for the period 1990 to 2018, with seasonality removed. Also shown is linear trend patterns of ERA5-Land (c), BARRA (d) and ERA5 (e) monthly mean soil moisture at their native resolution during the growing season for the deseasoned period 1990 to 2018. Stippling indicates significance at the 5% level within individual grid cells.

Soil moisture trends show agreement across all datasets, with declines throughout much of the country (Fig. 5; average country wide declines of 0.13 mm per growing season). Significant declines occur throughout the lower inner montane regions of the South Island and parts of the bottom of the country, while both BARRA and ERA5-Land reveal further significant declines throughout the north east and west of the South Island and the lower southeast and parts of the west coast of the North Island, which are strongest within the BARRA dataset. Broad agreement across datasets occurs with increased soil moisture across the upper North Island (not significant). ERA5-Land and ERA5 both reveal similar spatial patterns to changes in soil moisture, while BARRA indicates opposite signs of soil moisture patterns throughout the bottom and upper east coast of the North Island (decrease/increase in BARRA, increase/decrease in ERA5-Land and ERA5).

SM-P correlation (Kendall's $\tau$) shows good agreement across all reanalysis datasets, with statistically significant positive correlations across the entire country (Fig. 6; country average of 0.42 across all three reanalysis datasets). SM-T correlation also shows broad agreement between datasets (country wide average of -0.24 across all three reanalysis datasets). Significant negative correlations are found across all reanalysis datasets for much of the South Island and the lower North Island. The strongest coupling is found throughout the lower inner montane regions of the South Island, similar across all reanalysis datasets. The upper North Island displays positive correlation between soil moisture and temperature (significant in BARRA), represented across all reanalysis datasets, while this positive correlation extends into the middle reaches of the North Island within the BARRA dataset.

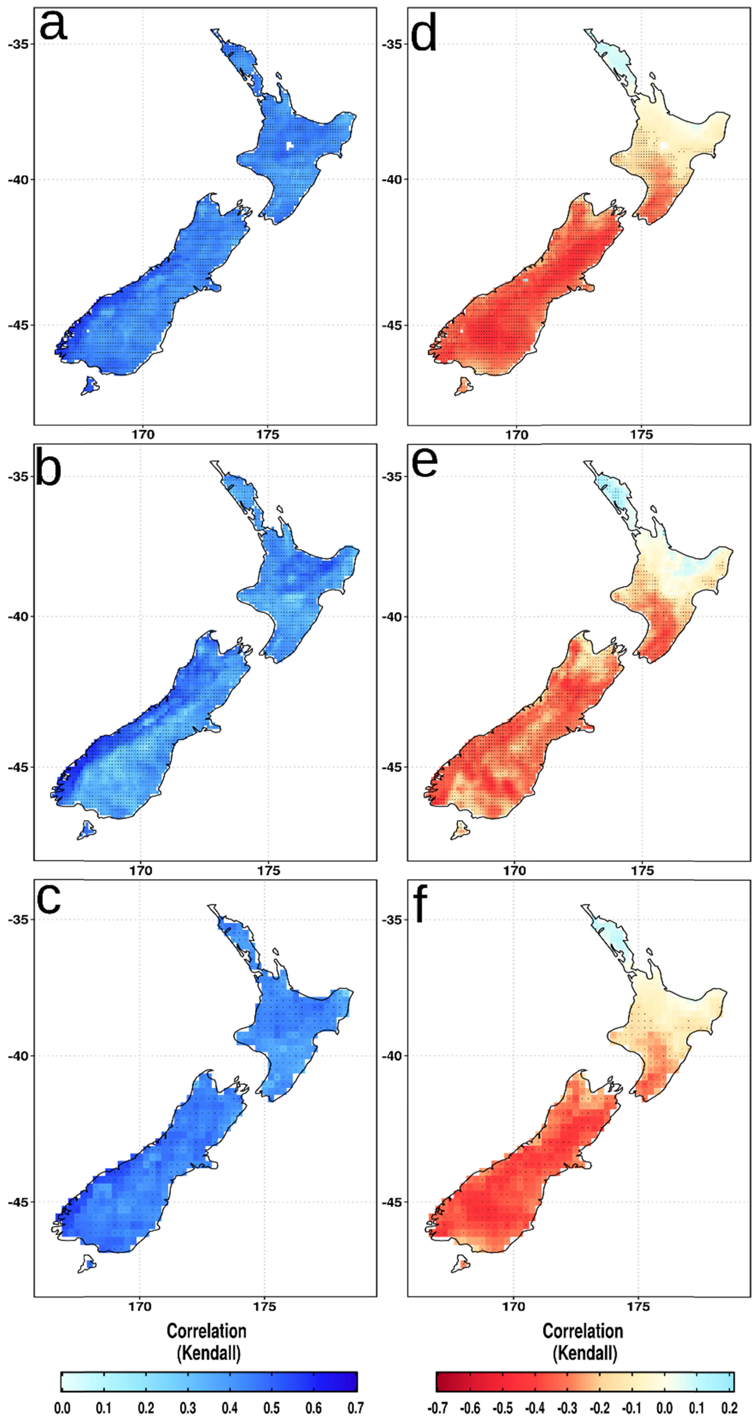


**Fig. 6** Monthly soil moisture correlation, represented by SM-P (a-c) and SM-T (d-f), showing ERA5-Land (a,d), BARRA (b,e) and ERA5 (c,f). Total precipitation and mean temperature are represented as VCSN data, aggregated to each datasets native resolution. Period shown is growing seasons (Nov-Mar) from 1990 to 2018, with seasonality removed. Stippling indicates significance at the 5% level within individual grid cells.

Good agreement in correlation strength is found amongst the datasets for both the dry and wet seasons. SM-P correlation during dry seasons shows widespread significant coupling across the entire country (country average of 0.32 across all three reanalysis datasets), with the strongest correlations across the south and west coast of the South Island (ERA5 and ERA5-Land) and lower east coast of the North Island (Fig. 7). Such a pattern is similarly replicated during the wet season (Fig. 8; country average of 0.30 across all three reanalysis datasets). Significant negative SM-T correlations are again present across much of the country during both the dry and wet seasons (country of average of -0.10/-0.08 across all three reanalysis datasets for dry/wet seasons), with the exception of the upper South Island and most of the top half of the North Island, similar across all reanalysis datasets. BARRA highlights positive SM-T correlation across these areas during the dry season. The emergence of these regions with positive SM-T correlations is stronger (and in agreement across all datasets) during the wet season, excluding the upper South Island.

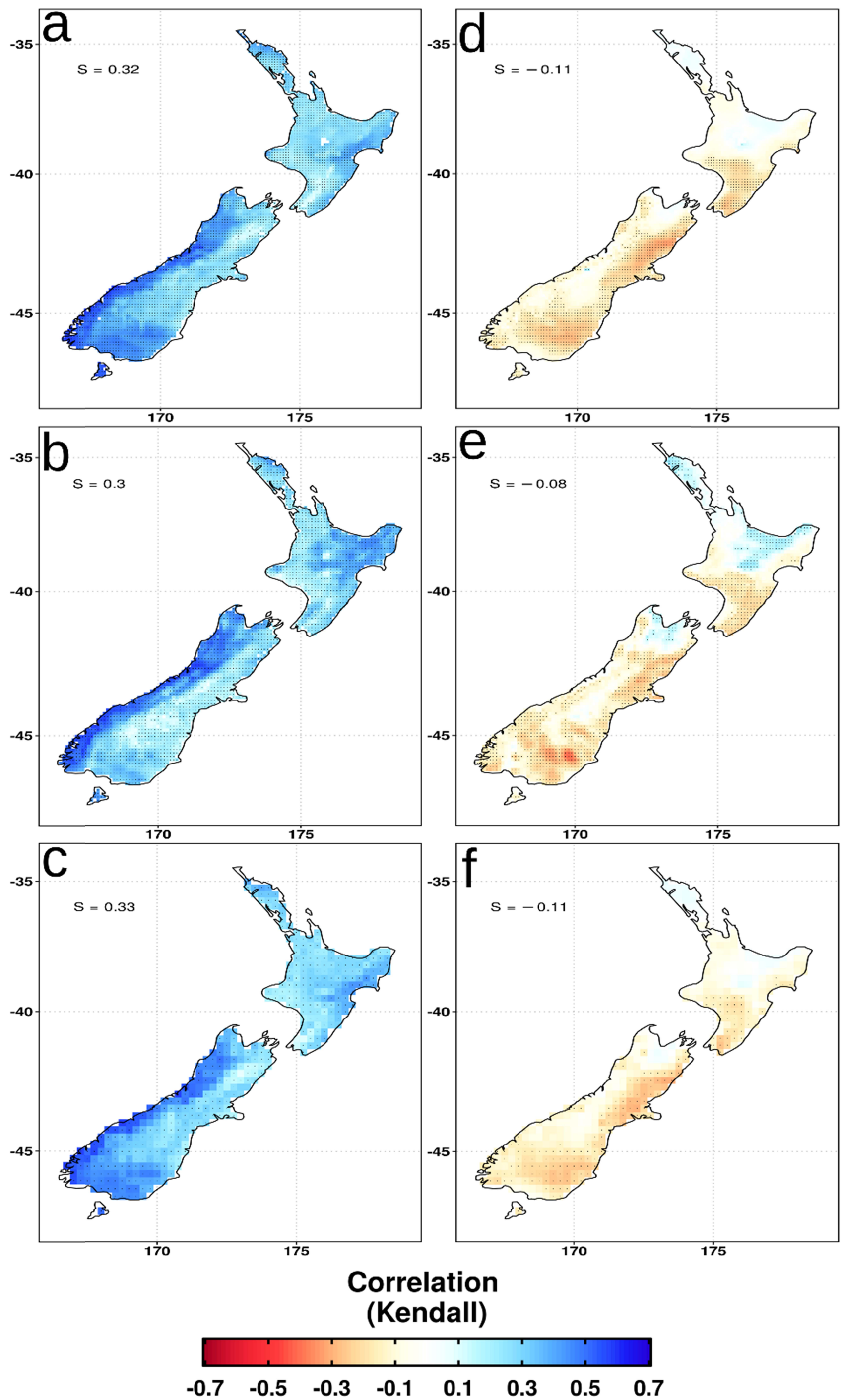


**Fig. 7** Dry season (as defined by bottom third of ranked monthly mean soil moisture, dataset specific) SM-P (a-c) and SM-T (d-f) correlation across reanalysis datasets (ERA5-Land (a,d); BARRA (b,e); ERA5 (c-f)) for the period January 1990 to December 2018. Total precipitation and mean temperature are represented as VCSN data, aggregated to each datasets native resolution. All data have had seasonality removed. Stippling indicates significance at the 5% level within individual grid cells. S represents mean spatial correlation.

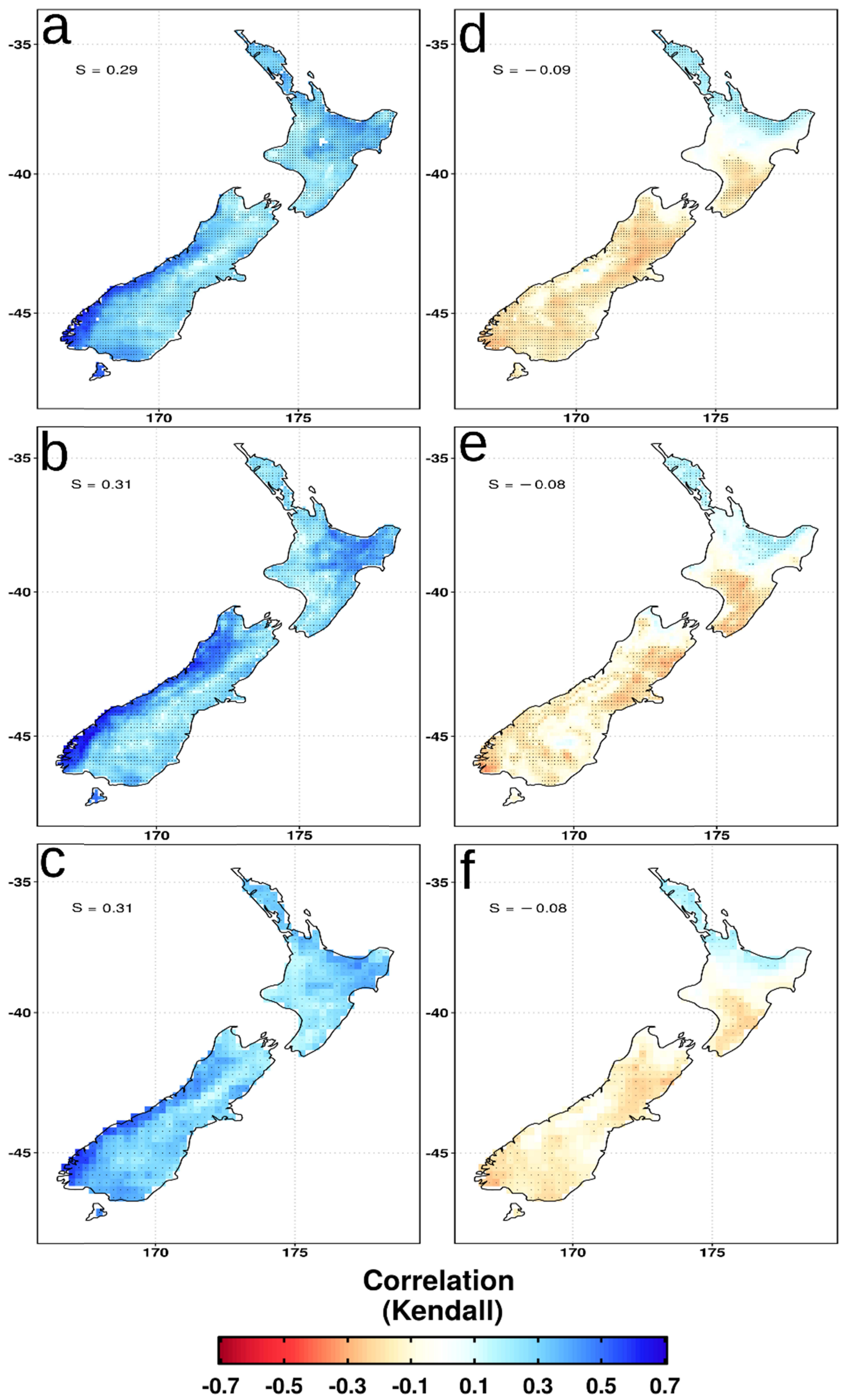


**Fig. 8** Wet season (as defined by top third of ranked monthly mean soil moisture, dataset specific) SM-P (a-c) and SM-T (d-f) correrlation across reanalysis datasets (ERA5-Land (a,d); BARRA (b,e); ERA5 (c-f)) for the period January 1990 to December 2018. Total precipitation and mean temperature are represented as VCSN data, aggregated to each datasets native resolution. All data have had seasonality removed. Stippling indicates significance at the 5% level within individual grid cells. S represents mean spatial correlation.

### 3.3. Compound and Seesaw Events

The co-occurrence of hot and dry extremes agrees strongly across the reanalysis datasets (Fig. 9). Areas of the lower and upper South Island reveal the most frequent occurrences of hot and dry conditions, with a maximum of 35 months across for the entire time series (10%) . BARRA also shows a large number of occurrences around the lower middle reaches of the North Island, which is not replicated in ERA5-Land and ERA5, one of the few deviations between datasets. Relatively few occurrences of hot and dry conditions exist across the upper and upper middle sections of the North Island.

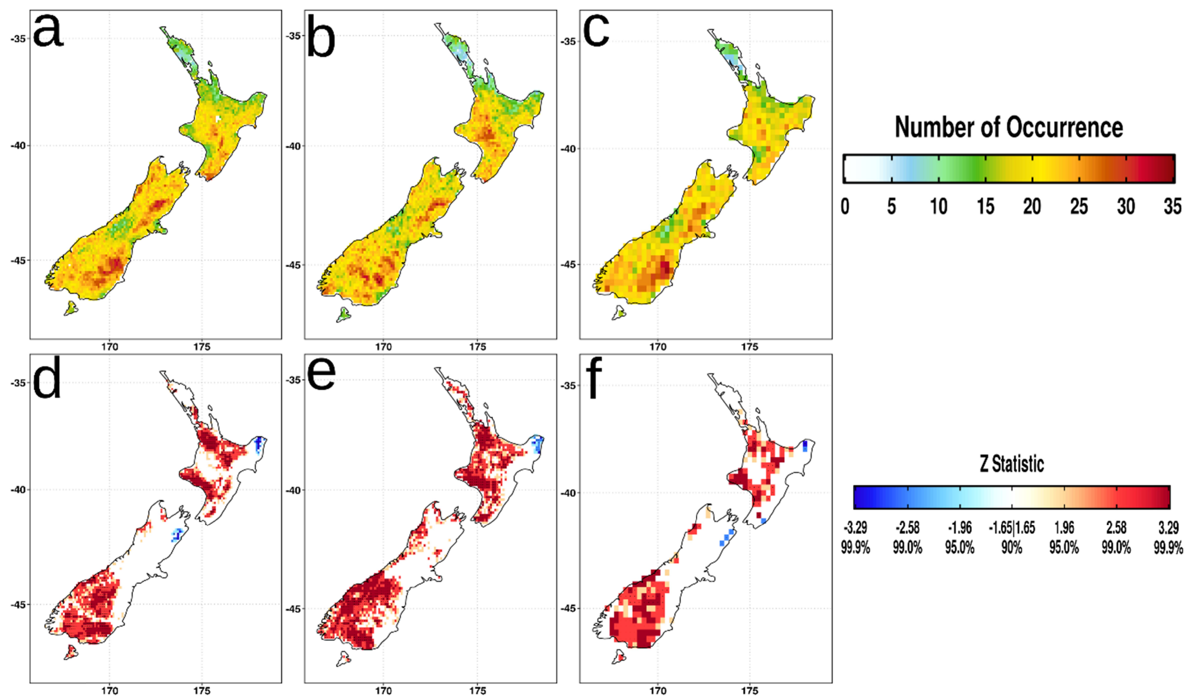


**Fig. 9** Co-occurrence of hot and dry months across New Zealand for the period January 1990 to December 2018, as represented by reanalysis datasets (ERA5-Land (a,d); BARRA (b,e); ERA5 (c-f)). The top row (a-c) signifies the number of months where hot (=> 1 of the STI) and dry (<= -1 of the SSMI) events co-occur, while the bottom row (d-f) indicates the trend of co-occurrence, calculated using Mann-Kendall. Stippling indicates those land grid cells with statistical significance under the Mann-Kendall test statistic at the 5% level.

Strong statistically significant increases in the co-occurrence of hot and dry months are present across the west coast, south and lower inner montane regions of the South Island, with significant increases also found across much of the east coast and middle reaches of the North Island (Fig. 9). This spatial coverage agrees across all reanalysis datasets. All reanalysis datasets agree in direction with regards to decreasing trends in hot and dry months in the north east regions of both islands, although this is not statistically significant for BARRA across the north east of the South Island.

Agreement in the representation of seesaw events (droughts which are followed by pluvials within one month; as a percentage) is present across all reanalysis datasets in the lower east coast regions of the South Island (25%-35%) and the Southern Alps (15%-25%) during the summer period, while during the winter period agreement is present throughout the lower South Island (25%-35%). Significant event occurrence (Poisson-based) across the upper east coast of the South Island agrees across all datasets during winter, although this is weaker in BARRA, with ERA5 and ERA5-Land also being significant during summer and the full time series. The middle reaches of the North Island contain significant event occurrences throughout all datasets and periods (15%-35%), except for the ERA5 full time series.

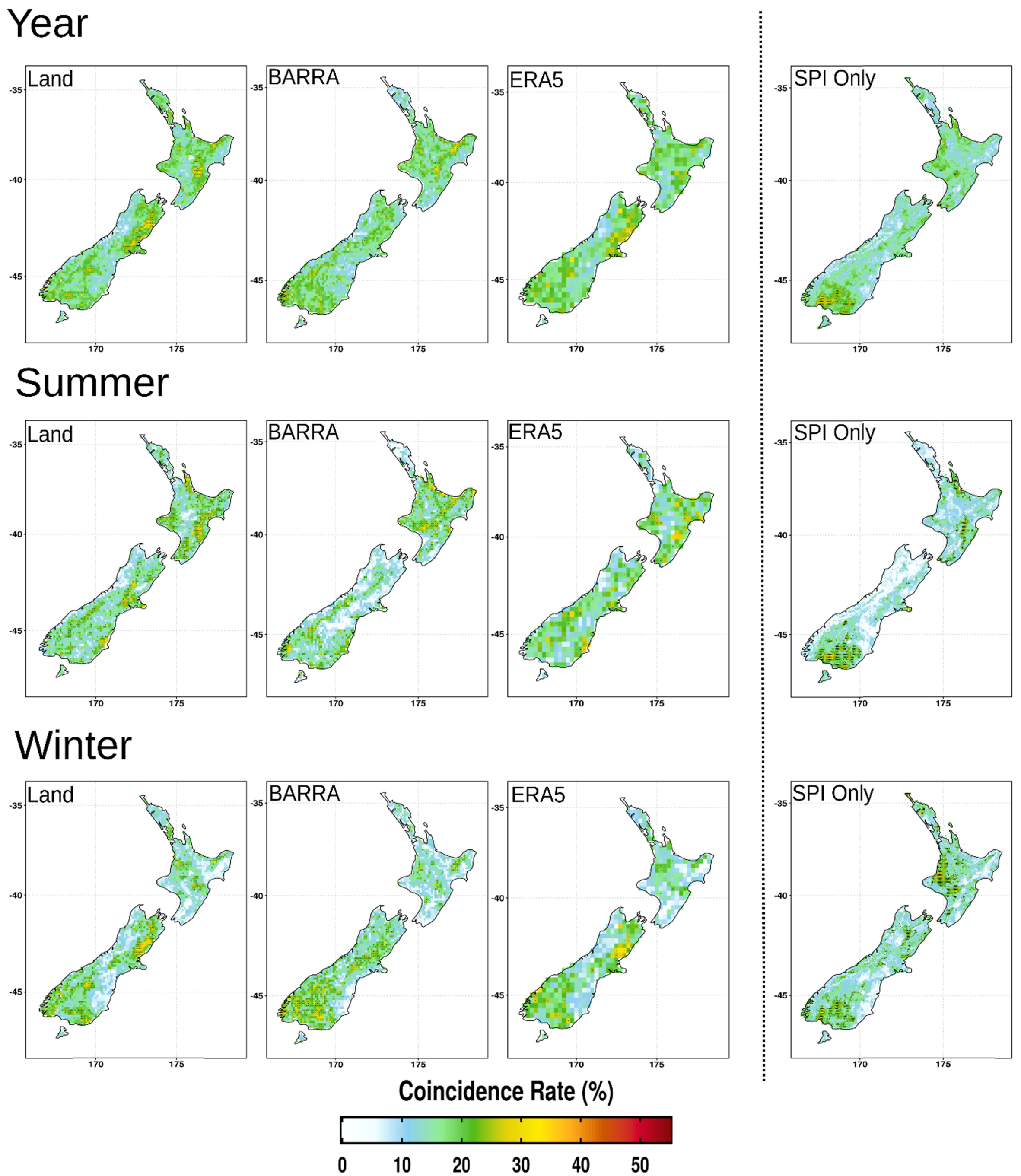


**Fig. 10** Seesaw events, calculated using the methodology of He and Sheffield (2020) and Siegmund *et al*. (2017). Depiction is of the percentage of droughts which are followed by pluvials at each grid cell, for each reanalysis dataset, using a one-month delay. Periods have been broken into an extended winter (Apr-Sep) and summer (Oct-Mar), while droughts are defined as below -1 on the SSMI and pluvials above 1 on the SPI. The far right column shows precipitation-based definitions of droughts and pluvials (i.e. defined as above/below -1/1 in the SPI). Stippling indicates significance according to the Poisson process-based significance test (Siegmund *et al*., 2017).

In comparison to seesaw events defined by SSMI droughts, seesaw events defined by SPI droughts show agreement across the south and north east of the South Island during winter periods. In contrast, the south of the South Island reveals significant seesaw event occurrence when droughts are defined using the SPI during summer periods and across the full time series, which is not present with SSMI defined droughts. During winter, the west coast of the North Island reveals a similar contrast between SSMI and SPI defined droughts.

## 4. Discussion

### 4.1. Comparison to Soil Moisture Observations

No substantial differences are detected between the three reanalysis soil moisture datasets (ERA5-Land, BARRA and ERA5). In particular, no dataset offers a better performance when compared to station observations (median correlation range of 0.02), nor does any spatial agreement become apparent (Fig. 4; Table 3). The similar performance of BARRA to both ERA5-Land and ERA5 indicates that the assimilation of local station observations into the model does not result in significant improvements in the representation of soil moisture, despite the greater accuracy in the representation of both precipitation and temperature for New Zealand within BARRA (Pirooz *et al.*, 2021) and the good skill in soil moisture representation within the underlying JULES land surface model (Yang *et al.*, 2014). This absence of any significant improvement in BARRA indicates that the performance increases seen in ERA5 Land (increased resolution) and ERA5 (satellite assimilation) may be of more significance to increased soil moisture representation skill than assimilation of primary variables from local station observations.

Minor improvements in the representation of ERA5 soil moisture compared to observations (mean of all locations) across New Zealand are apparent, particularly relating to the ability to capture the temporal trends and anomalies (Table 2; correlations of 0.80 and 0.84 respectively). Within the ERA5 land-surface model, soil moisture is corrected via the use of assimilated satellite observations (de Rosnay *et al.*, 2014), resulting in improvements compared to previous generation reanalysis products globally (Li *et al.*, 2020). Of note, the ERA5-Land dataset does not benefit from this assimilation process (Beck *et al.*, 2021).

The lack of improvement between ERA5 and ERA5 Land for soil moisture representation in the current work stands in contrast to the improvements found between ERA5 and ERA5 Land that was achieved via an increase in model resolution (Beck *et al*., 2021; Muñoz-Sabater *et al.*, 2019), although the differences in skill are minor (Fig. 2; Table 2; average correlation difference of 0.05). The performance of ERA5-Land in capturing the complexity in soil moisture characteristics and terrain for New Zealand (Hewitt, 2010; Salinger and Mullan, 1999) when downscaled to a fine resolution, itself embedded within the uncertainties of comparing point based with grid scale measurements (Li *et al.*, 2020), may explain these minor differences. Therefore, the improvements in soil moisture representation via assimilated satellite observations revealed here (Fig. 3; Table 2) provide important findings for the continued advances in regional scale reanalysis products (Su *et al.*, 2021) and the proposed New Zealand Reanalysis (NZRA; Pirooz *et al.*, 2021). Advancements of regional and local reanalysis soil moisture products may therefore be further improved via the use of local climate data assimilation together with satellite assimilation of soil moisture observations. Despite the inability of the three reanalysis datasets to capture the observed soil moisture trend (0.56 mm $yr^{-1}$), the accurate portrayal of extreme events and the seasonal cycle in soil moisture, emphasised as the true value in soil moisture representation by Koster *et al*. (2009), make all three reanalysis soil moisture datasets worthwhile additions to any investigation of extreme hydrometeorological events (Fig. 3; Table 2).

## 4.2. Land-Atmosphere Coupling

Trends in both growing season precipitation and temperature (1990-2018) are similar to those summer temperature and precipitation increases reported both nationally (Mullan *et al*., 2010) and internationally (IPCC, 2021), with a mean growing season (November-March) temperature increase (precipitation decrease) of 0.04°C (0.61 mm). Here, trends in soil moisture (1990-2018), ranging from -0.51 to +0.17 mm per growing season (mean -0.13 mm), are reported for the first time for New Zealand. The declines in soil moisture across much of the South Island and lower North Island (Fig. 5) closely resemble the widespread negative correlation between soil moisture and temperature (Fig. 6). The close spatial agreement between SM-T correlation and soil moisture declines, embedded within country-wide growing season temperature increases, reinforces the importance of soil moisture and land-atmosphere coupling, even for temperate/maritime climate zones. Meanwhile, the strong correlation between soil moisture and precipitation is typical of a maritime climate (Sehler *et al.*, 2019).

Areas of positive SM-T correlation exist across the upper North Island in the BARRA dataset (Fig. 7) while during the wet season these areas become significantly positively correlated (SM-T) within all datasets (Fig. 8), highlighting the regional differences in atmospheric drivers of soil moisture. With relatively minor precipitation changes across growing seasons, the emergence of soil moisture declines, together with the strong correlation within SM-T relationships, further evidences the importance of SM-T coupling for New Zealand. The strong SM-T coupling during the growing season indicates a phase change in land states for these typically wet regions during dry seasons, revealing potential "hot spot" areas of land-atmosphere coupling like that witnessed during the 2018 summer drought and heatwave across the wet, energy-limited regions of Northern Europe and the United Kingdom (Dirmeyer *et al*., 2021; Orth, 2021).

As noted by Berg and Sheffield (2018), soil moisture proxy metrics (such as the Standardised Precipitation and Evapotranspiration Index (SPEI) and Potential Evapotranspiration Deficit (PED)) indicate dramatic increases in future global drought severity, in contrast to trends in the soil moisture outputs from modelled land-atmosphere systems. Berg and Sheffield (2018) suggest that the soil moisture-vegetation-atmosphere coupling, inherent in land-atmosphere models, explains this discrepancy via the representation of AET over PET, and calls for the assessment of droughts using these model outputs rather than offline proxy metrics.

Importantly, the land-atmosphere coupling which Berg and Sheffield (2018) suggests may explain drought projection discrepancies (via complex soil moisture-energy flux feedbacks) exists in the current work (Fig. 6; Fig. 7; Fig. 8). Projections of drought risk for New Zealand indicate increased drought risk across the country under various Representative Concentration Pathway (RCP) scenarios (Mullan *et al.*, 2018), while historical soil moisture changes have also highlighted increased drought risk (Ministry for the Environment and Statistics New Zealand, 2020; Porteous and Mullan, 2013). These drought projections and investigations in a New Zealand context have involved offline projections using soil moisture proxy metrics such as the SPEI and PED, with reported soil moisture declines in excess of those present here (Porteous and Mullan, 2013). Therefore, previous assessments of drought across New Zealand would benefit from a careful re-evaluation using coupled soil moisture products.

### 4.3. Compound and Seesaw Events

With the correlation between soil moisture and temperature during growing seasons in mind (Fig. 6), the spatial agreement with compounding hot and dry months (Fig. 9) suggests soil moisture drought (dry) plays some combination of roles as a driver and/or outcome of heat wave occurrence (hot). An ever-growing body of research internationally (Hao *et al.*, 2020; Zscheischler *et al.*, 2018; Wu *et al.*, 2021) indicates the substantial negative impact these co-occurring, or compounding, events can have. With the current work revealing such compounding effects are present throughout New Zealand (maximum occurrence of hot and dry conditions occurring 10% of the time between 1990-2018), further work is urgently required in exploring the role heat waves may play in the onset of flash droughts (Mo and Lettenmaier, 2015), or the role drought may play in priming the land surface for heat wave onset (Dirmeyer *et al.*, 2021).

While a relatively cool climate, heat waves in a New Zealand context have recently come under increased scrutiny, with developments highlighting the importance of relative heat (Harrington, 2021) and the role of sea surface temperatures on atmospheric conditions (Salinger *et al.*, 2019). In particular, heat wave risk has shown to have strong regional variation under temperature increases (Harrington and Frame, 2022). The low occurrence of compound hot and dry conditions across the upper north and northeast of the North Island (Fig. 9) sits in contrast to the increase in hot days found by Harrington (2021), while the high number of compounding months sits somewhat more in agreement spatially to hot day occurrence. The discrepancy suggests that soil moisture plays a less important role in compound event occurrence across the upper north and northeast of the North Island which results in a more stable land state during dry phases (Orth, 2021), particularly when viewed collectively with the weak to positive covariation in SM-T throughout these typically wet or transitional regions (Fig. 6).

Modest frequency of seesaw event occurrence (i.e. on average 17% of droughts are followed by pluvial activity the following month) is found in the present work, like that found globally by He and Sheffield (2020). This modest occurrence may in part reflect the approach of He and Sheffield (2020) in creating binary event occurrence for seesaw event detection, resulting in a loss of information as a result of the strict detection criteria. SPI-defined drought identify a greater occurrence of seesaw events than SSMI-defined drought throughout the west coast of the North Island (winter) and lower South Island (summer), due to the one-month accumulation period being unable to capture the persistent nature of soil moisture droughts (Hao and AghaKouchak, 2013). In contrast, the stronger seesaw event occurrence under SSMI droughts during winter in the north-east of the South Island indicates a strong persistence of drought conditions throughout the region that is not captured by the SPI, highlighting the complicated dynamics of regional differences in land surface interactions and the propagation of drought through the hydrological cycle. Investigating these seesaw event occurrences requires further exploration, particularly relating to an exploration of the temporal delay to capture seasonal cycles (He and Sheffield, 2020).

The rapid transition from dry to wet during seesaw events implies substantial and/or persistent precipitation events. In New Zealand, Reid *et al.* (2021) identified that eight (Christchurch and New Plymouth) and nine (Dunedin) of the top ten rainfall events were associated with an atmospheric river; narrow bands of intense water vapour transport (Newell *et al.*, 1992) that have becoming increasingly associated with extreme precipitation and flooding across New Zealand (Prince *et al*., 2021; Shu *et al.*, 2021). These same sites (Christchurch, New Plymouth and Dunedin) simultaneously reveal high occurrence of seesaw events in the present work (Fig. 10). Further, Reid *et al.* (2021) identified a strong seasonal cycle in atmospheric river occurrence, with over 60% of events occurring during the warm period (January – April), with high seesaw event occurrence during the summer phase also revealed in the present work (Fig. 10). The presence of strong seesaw event occurrence in similar regions to those that experience frequent atmospheric rivers (Prince *et al*., 2021; Reid *et al*., 2021) suggests the possibility of "drought buster" behaviour associated with atmospheric rivers (Dettinger, 2013). While the present study indicates preliminary findings of seesaw event behaviour for New Zealand, a more focused investigation is needed, including understanding the role atmospheric rivers play during this transitional phase.

## 5. Conclusion

For regions with physically diverse landscapes such as New Zealand, the increased resolution of current generation reanalysis datasets makes them an increasingly attractive option for climatological and hydrological analysis. The ability of the reanalysis datasets here to capture the seasonal cycle and residual anomalies highlights the strong utility reanalysis soil moisture products have, particularly considering the real value in soil moisture data exists in its time variability rather than the representation of absolute magnitudes. With existing soil moisture data across New Zealand often employing as an offline proxy metric, the ability of the current generation products to capture the soil moisture cycles and coupling regimes, is a key benefit. The results here indicate good agreement in the representation of soil moisture in the three investigated reanalysis datasets for the period 1999-2018 (ERA5 Land, BARRA and ERA5; correlation range of 0.03). While trends in soil moisture are unable to be adequately captured by reanalysis products (mean of 0.08 mm $yr^{-1}$ compared to 0.56 mm $yr^{-1}$ in observations), the performance must be considered relative to the difficulties of comparing point based and grid cell data, while the agreement in seasonal cycle (correlations of 0.97-0.99) and ability to capture anomalies (correlations of 0.79-0.84) of the reanalysis dataset are promising. For the extended period 1990-2018, mean (ERA5 Land, BARRA and ERA5), New Zealand wide declines in growing season soil moisture of 0.13 mm are reported for the first time.

Land-atmosphere coupling in a New Zealand context is poorly understood, with land variation often assumed to be driven by precipitation interactions. While clearly playing a significant role, the interaction of SM-T correlations reveals key areas of the country where soil moisture responds strongly to temperature variation. Spatially, the increased strength of the correlation between soil moisture and temperature matches the reported temperature increase (0.04 °C per growing season), with important implications under projected temperature increases. Further work should be directed towards a detailed investigation involving heat and energy fluxes to unravel the role soil moisture plays on temperature in a New Zealand context. Examining changes in drought (via soil moisture) behaviour under a changing climate using these coupled products would be insightful, particularly when compared to the soil moisture proxy metrics traditionally employed in a New Zealand context.

For the first time, compounding and seesaw events are examined in a New Zealand context, reflecting the turn in focus in the international research community. With regards to compound events, the present study highlights large portions of the country where compounding hot and dry conditions occur (maximum occurrence of 10% across the time period 1990-2018), including key agricultural areas where traditional energy-limited regimes appear to reveal a shift to a dry, water limited state. Taken collectively with the previously revealed SM-T relationship, the historical increase in these hot and dry conditions has important implications for the understanding of land responses to atmosphere changes under a continuing changing climate. The present work also indicates the potential role atmospheric river events may play during the seesaw phase of

New Zealand's climate, with an average of 17% of droughts being followed by pluvial activity (1990-2018), highlighting a worthy new direction for atmospheric river research in New Zealand. Collectively, the present work has provided a preliminary look at compounding and seesaw event behaviour across New Zealand, revealing both areas to be a promising avenue for future research.

## Acknowledgements

VCSN data was kindly supplied by NIWA (Gregor Macara and Andrew Tait). A University of Otago Doctoral Scholarship supported the lead author in the preparation of this manuscript.

## Supporting Information

**Table S1** Information on station locations and associated AWS

**Fig. S1** Methodological framework employed in the current work, offering a graphical representation of the steps employed in Sections 2.1.2 through 2.4.

## References

Beck, H., Pan, M., Miralles, D., Reichle, R., Dorigo, W., Hahn, S., Sheffield, J., Karthikeyan, L., Balsamo, G., Parinussa, R., van Dijk, A., Du, J., Kimball, J., Vergopolan, N. and Wood, E. (2021). Evaluation of 18 satellite-and model-based soil moisture products using in situ measurements from 826 sensors. *Hydrology and Earth System Sciences*, *25* (1), 17–40.

Bennet, M. and Kingston, D. (2022). Spatial patterns of atmospheric vapour transport and their connection to drought in New Zealand. *International Journal of Climatology*, 1–21.

Berg, A. and Sheffield, J. (2018). Climate Change and Drought: the Soil Moisture Perspective. *Current Climate Change Reports*, *4* (2), 180–191.

Chen, L. and Dirmeyer, P. (2020). Distinct Impacts of Land Use and Land Management on Summer Temperatures. *Frontiers in Earth Science*, *8* (245), 1–12.

Cleveland, R., Cleveland, W., McRae, J. and Terpenning, I. (1990). STL: A Seasonal-Trend Decomposition Procedure Based on Loess. *Journal of Official Statistics*, *6* (1), 3–73.

CliFlo - National Institute of Water and Atmospheric Research (NIWA): The National Climate Database. (2021). https://cliflo.niwa.co.nz/. Accessed: 2021- 11-15.

de Rosnay, P., Balsamo, G., Albergel, C., Muñoz-Sabater, J. and Isaksen, L. (2014). Initialisation of Land Surface Variables for Numerical Weather Prediction. *Surveys in Geophysics*, *35* (3), 607–621.

Dettinger, M. (2013). Atmospheric Rivers as Drought Busters on the U.S. West Coast. *Journal of Hydrometeorology*, *14* (6), 1721–1732.

Dirmeyer, P., Balsamo, G., Blyth, E., Morrison, R. and Cooper, H. (2021). Land-Atmosphere Interactions Exacerbated the Drought and Heatwave Over Northern Europe During Summer 2018. *AGU Advances*, *2* (2), 1–16.

Donat, M., Lowry, A., Alexander, L., O'Gorman, P. and Maher, N. (2016). More extreme precipitation in the world's dry and wet regions. *Nature Climate Change*, *6* (5), 508–513.

Feng, S., Hao, Z., Wu, X., Zhang, X. and Hao, F. (2021). A multi-index evaluation of changes in compound dry and hot events of global maize areas. *Journal of Hydrology*, *602* (1), 126728–126736.

Ferguson , C. and Wood, E. (2011). Observed land-atmosphere coupling from satellite remote sensing and reanalysis. *Journal of Hydrometeorology, 12* (6), 1221-1254.

Ficklin, D., Null, S., Abatzoglou, J., Novick, K. and Myers, D. (2022). Hydrological Intensification Will Increase the Complexity of Water Resource Management. *Earth's Future*, *10* (3), 1–16.

Fischer, E., Seneviratne, S., Lüthi, D. and Schär, C. (2007). Contribution of land- atmosphere coupling to recent European summer heat waves. *Geophysical Research Letters*, *34* (6), 1–6.

Gentine, P., Massmann, A., Lintner, B., Hamed Alemohammad, S., Fu, R., Green, J., Kennedy, D. and Vilà-Guerau de Arellano, J. (2019). Land-atmosphere interactions in the tropics - a review. *Hydrology and Earth System Sciences*, *23* (10), 4171–4197.

Gevaert, A., Miralles, D., de Jeu, R., Schellekens, J. and Dolman, A. (2018). Soil Moisture- Temperature Coupling in a Set of Land Surface Models. *Journal of Geophysical Research: Atmospheres*, *123* (3), 1481–1498.

Gruber, A., De Lannoy, G., Albergel, C., Al-Yaari, A., Brocca, L., Calvet, J., Colliander, A., Cosh, M., Crow, W., Dorigo, W., Draper, C., Hirschi, M., Kerr, Y., Konings, A., Lahoz, W., McColl, K., Montzka, C., Muñoz-Sabater, J., Peng, J., Reichle, R., Richaume, P., Rüdiger, C., Scanlon, T., van der Schalie, R., Wigneron, J. and Wagner, W. (2020). Validation practices for satellite soil moisture retrievals: What are (the) errors? *Remote Sensing of Environment*, *244* (1), 111806–111839.

Hao, Z. and AghaKouchak, A. (2013). Multivariate Standardized Drought Index: A parametric multi-index model. *Advances in Water Resources*, *57* (1), 12–18.

Hao, Z. and AghaKouchak, A. (2014). A Nonparametric Multivariate Multi-Index Drought Monitoring Framework. *Journal of Hydrometeorology*, *15* (1), 89–101.

Hao, Z., Hao, F., Singh, V., Ouyang, W., Zhang, X. and Zhang, S. (2020). A joint extreme index for compound droughts and hot extremes. *Theoretical and Applied Climatology*, *142* (1), 321–328.

Harrington, L. (2021). Rethinking extreme heat in a cool climate: a New Zealand case study. *Environmental Research Letters*, *16* (3), 1–10.

Harrington, L. and Frame, D. (2022). Extreme heat in New Zealand: a synthesis. *Climatic Change*, 1–19 (under review).

He, X. and Sheffield, J. (2020). Lagged Compound Occurrence of Droughts and Pluvials Globally Over the past Seven Decades. *Geophysical Research Letters*, *47* (14), 101029– 101043.

Hersbach, H., Bell, B., Berrisford, P., Hirahara, S., Horányi, A., Muñoz-Sabater, J., Nicolas, J., Peubey, C., Radu, R., Schepers, D., Simmons, A., Soci, C., Abdalla, S., Abellan, X., Balsamo, G., Bechtold, P., Biavati, G., Bidlot, J., Bonavita, M., De Chiara, G., Dahlgren, P., Dee, D., Diamantakis, M., Dragani, R., Flemming, J., Forbes, R., Fuentes, M., Geer, A., Haimberger, L., Healy, S., Hogan, R., Hólm, E., Janisková, M., Keeley, S., Laloyaux, P., Lopez, P., Lupu, C., Radnoti, G., de Rosnay, P., Rozum, I., Vamborg, F., Villaume, S. and Thépaut, J. (2020). The ERA5 global reanalysis. *Quarterly Journal of the Royal Meteorological Society*, *146* (730), 1999–2049.

Hewitt, A. (2010). *New Zealand Soil Classification* (3rd ed.). 136 pp. Lincoln, New Zealand: Manaaki Whenua Press.

IPCC. 2021. *Climate Change 2021: The Physical Science Basis. Contribution of Working Group I to the Sixth Assessment Report of the Intergovernmental Panel on Climate Change*. In Masson-Delmotte, V., Zhai, P., Pirani, A., Connors, S., Péan, C., Berger, S., Caud, N., Chen, Y., Goldfarb, L., Gomis, M., Huang, M., Leitzell, K., Lonnoy, E., Matthews, J., Maycock, T., Waterfield, T., Yelekçi, O., Yu, R. and Zhou, B. (Eds.), *Sisth Assessment Report of the Intergovernmental Panel on Climate Change (IPCC)* (pp. 1–2409). Cambridge, United Kingdom: Cambridge University Press.

Jiao, D., Xu, N., Yang, F. and Xu, K. (2021). Evaluation of spatial-temporal variation performance of ERA5 precipitation data in China. *Scientific Reports*, *11* (1), 1–13.

Kao, S. and Govindaraju, R. (2010). A copula-based joint deficit index for droughts. *Journal of Hydrology*, *380* (1), 121–134.

Kendall, M. (1938). A new measure of rank correlation. *Biometrika*, *30* (1), 81–93.

Knist, S., Goergen, K., Buonomo, E., Christensen, O., Colette, A., Cardoso, R., Fealy, R., Fernández, J., García-Díez, M., Jacob, D., Kartsios, S., Katragkou, E., Keuler, K., Mayer, S., van Meijgaard, E., Nikulin, G., Soares, P., Sobolowski, S., Szepszo, G., Teichmann, C., Vautard, R., Warrach-Sagi, K., Wulfmeyer, V. and Simmer, C. (2017). Land-atmosphere coupling in EURO-CORDEX evaluation experiments. *Journal of Geophysical Research: Atmospheres*, *122* (1), 79–103.

Koster, R., Guo, Z., Yang, R., Dirmeyer, P., Mitchell, K. and Puma, M. (2009). On the Nature of Soil Moisture in Land Surface Models. *Journal of Climate*, *22* (16), 4322–4235.

Li, H., Robock, A., Liu, S., Mo, X. and Viterbo, P. (2005). Evaluation of Reanalysis Soil Moisture Simulations Using Updated Chinese Soil Moisture Observations. *Journal of Hydrometeorology*, *6* (2), 180–193.

Li, M., Ma, Z., Gu, H., Yang, Q. and Zheng, Z. (2017). Production of a combined land surface data set and its use to assess land-atmosphere coupling in China. *Journal of Geophysical Research: Atmospheres*, *122* (2), 948–965.

Li, M., Wu, P. and Ma, Z. (2020). A comprehensive evaluation of soil moisture and soil temperature from third-generation atmospheric and land reanalysis data sets. *International Journal of Climatology*, *40* (13), 5744–5766.

Ling, X., Huang, Y., Guo, Y., W. Wang, Chen, C., Qiu, B., Ge, J., Qin, K., Xue, Y. and Peng, J. (2021). Comprehensive evaluation of satellite-based and reanalysis soil moisture products using in situ observations over China. *Hydrology and Earth System Sciences*, *25* (7), 4209–4429.

Macara, G. (2018). *The Climate and Weather of New Zealand*. National Institute of Water and Atmospheric Research Ltd. 52 pp. Wellington, New Zealand.

Mann, H. (1945). Nonparametric Tests Against Trend. *Econometrica*, 13 (3), 245-259.

Manning, C., Widmann, M., Bevacqua, E., Van Loon, A., Maraun, D. and Vrac, M. (2019). Increased probability of compound long-duration dry and hot events in Europe during summer (1950-2013). *Environmental Research Letters, 14* (9), 94006-94022.

McKee, T., Doesken, N. and Kleist, J. (1993). The relationship of drought frequency and duration to time scales, Anaheim, CA, U.S.A.: American Meteorological Society, 179–184. January 17-22.

Ministry for the Environment and Statistics New Zealand (2020). *Our atmosphere and climate 2020*. Ministry for the Environment and Statistics New Zealand. 84 pp. Wellington, New Zealand: Ministry for the Environment and Statistics New Zealand.

Mo, K. and Lettenmaier, D. (2015). Heat wave flash droughts in decline. *Geophysical Research Letters*, *42* (8), 2823–2829.

Moravec, V., Markonis, Y., Rakovec, O., Svoboda, M., Trnka, M., Kumar, R. and Hanel, M. (2021). Europe under multi-year droughts: how severe was the 2014-2018 drought period? *Environmental Research Letters, 16* (3), 34062-34074.

Mullan, A., Stuart, S., Hadfield, M. and Smith, M. (2010). *Report on the Review of NIWA's 'Seven-Station' Temperature Series*. National Institute of Water and Atmospheric Research Ltd. 175 pp. Wellington, New Zealand.

Mullan, B., Sood, A., Stuart, S. and Carey-Smith, T. (2018). *Climate Change Projections for New Zealand: Atmosphere Projections Based on Simulations from the IPCC Fifth Assessment*. National Institute of Water and Atmospheric Research. 131 pp. Wellington, New Zealand: Ministry for the Environment.

Muñoz-Sabater, J., Dutra, E., Agustí-Panareda, A., Albergel, C., Arduini, G., Balsamo, G., Boussetta, S., Choulga, M., Harrigan, S., Hersbach, H., Martens, B., Miralles, D., Piles, M., Rodríguez-Fernández, N., Zsoter, E., Buontempo, C. and Thépaut, J. (2021). ERA5-Land: A state-of-the-art global reanalysis dataset for land applications. *Earth System Science Data*, *13* (9), 4349–4383.

Muñoz-Sabater, J., Lawrence, H., Albergel, C., de Rosnay, P., Isaksen, L., Mecklenburg, S., Kerr, Y. and Drusch, M. (2019). Assimilation of SMOS brightness temperatures in the ECMWF Integrated Forecasting System. *Quarterly Journal of the Royal Meteorological Society*, *145* (723), 2524–2548.

Newell, R., Newell, N., Zhu, Y. and Scott, C. (1992). Tropospheric Rivers? - A Pilot Study. *Geophysical Research Letters*, *19* (24), 2401–2404.

Orth, R. (2021). When the Land Surface Shifts Gears. *AGU Advances, 2* (2), 1-4.

Pearson, K. (1895). Note on Regression and Inheritance in the Case of Two Parents. *Proceedings of the Royal Society of London*, *58* (352), 240–242.

Perkins-Kirkpatrick, S. and Lewis, S. (2020). Increasing trends in regional heatwaves. *Nature Communications*, *11* (1), 1–8.

Pirooz, A., Moore, S., Carey-Smith, T., Turner, R. and Su, C. (2021). Evaluation of global and regional reanalyses performance over New Zealand. *Weather and Climate*, *41* (1), 52–71.

Porteous, A. and Mullan, B. (2013). *The 2012-13 drought: an assessment and historical perspective*. Ministry for Primary Industries. 57 pp. Wellington, New Zealand.

Porteous, A., Basher, R. and Salinger, M. (1994). Calibration and performance of the single-layer soil water balance model for pasture sites. *New Zealand Journal of Agricultural Research*, *37* (1), 107–118.

Prince, H., Cullen, N., Gibson, P., Conway, J. and Kingston, D. (2021). A Climatology of Atmospheric Rivers in New Zealand. *Journal of Climate*, *34* (11), 4383–4402.

Rajulapati, C., Papalexiou, S., Clark, M. and Pomeroy, J. (2021). The Perils of Regridding: Examples using a Global Precipitation Dataset. *Journal of Applied Meteorology and Climatology*, 1561–1573.

Reid, K., Rosier, S., Harrington, L., King, A. and Lane, T. (2021). Extreme rainfall in New Zealand and its association with Atmospheric Rivers. *Environmental Research Letters*, *16* (4), 44012–44022.

Salinger, M. (1987). Impact of climatic warming on the New Zealand growing season. *Journal of the Royal Society of New Zealand*, *17* (4), 363–371.

Salinger, M. and Mullan, A. (1999). New Zealand climate: temperature and precipitation variations and their links with atmospheric circulation 1930-1994. *International Journal of Climatology*, *19* (10), 1049–1071.

Salinger, M., Renwick, J., Behrens, E., Mullan, A., Diamond, H., Sirguey, P., Smith, R., Trought, M., Alexander, L., Cullen, N., Fitzharris, B., Hepburn, C., Parker, A. and Sutton, P. (2019). The unprecedented coupled ocean-atmosphere summer heatwave in the New Zealand region 2017/18: drivers, mechanisms and impacts. *Environmental Research Letters*, *14* (4), 44023–44040.

Sehler, R., Li, J., Reager, J. and Ye, H. (2019). Investigating Relationship Between Soil Moisture and Precipitation Globally Using Remote Sensing Observations. *Journal of Contemporary Water Research and Education*, *168* (1), 106–118.

Seneviratne, S., Corti, T., Davin, E., Hirschi, M., Jaeger, E., Lehner, I., Orlowsky, B. and Teuling, A. (2010). Investigating soil moisture-climate interactions in a changing climate: A review. *Earth-Science Reviews*, *99* (3), 125–161.

Sheffield, J., Goteti, G., Wen, F. and Wood, E. (2004). A simulated soil moisture based drought analysis for the United States. *Journal of Geophysical Research*, *109* (24), 1–19.

Shu, J., Shamseldin, A. and Weller, E. (2021). The impact of atmospheric rivers on rainfall in New Zealand. *Scientific Reports*, *11* (1), 1–11.

Siegmund, J., Siegmund, N. and Donner, R. (2017). CoinCalc - A new R package for quantifying simultaneities of event series. *Computers and Geosciences*, *98* (1), 64–72.

Sivapalan, M., Blöschl, G., Merz, R. and Gutknecht, D. (2005). Linking flood frequency to long-term water balance: Incorporating effects of seasonality. *Weather and Climate Extremes*, *41* (6), 1–17.

Spinoni, J., Barbosa, P., Bucchignani, E., Cassano, J., Cavazos, T., Christensen, J., Christensen, O., Coppola, E., Evans, J., Geyer, B., Giorgi, F., Hadjinicolaou, P., Jacob, D., Katzfey, J., Koenigk, T., Laprise, R., Lennard, C., Kurnaz, M., Li, D., Llopart, M., McCormick, N., Naumann, G., Nikulin, G., Ozturk, T., Panitz, H., da Rocha, R., Rockel, B., Solman, S., Syktus, J., Tangang, F., Teichmann, C., Vautard, R., Vogt, J., Winger, K., Zittis, G. and Dosio, A. (2020). Future Global Meteorological Drought Hot Spots: A Study Based on CORDEX Data. *Journal of Climate*, *33* (9), 3635–3661.

Su, C., Eizenberg, N., Steinle, P., Jakob, D., Fox-Hughes, P., White, C., Rennie, S., Franklin, C., Dharssi, I. and Zhu, H. (2019). BARRA v1.0: the Bureau of Meteorology Atmospheric high-resolution Regional Reanalysis for Australia. *Geoscientific Model Development*, *12* (5), 2049–2068.

Su, C., Eizenberg, N., Jakob, D., Fox-Hughes, P., Steinle, P., White, C. and Franklin, C. (2021). BARRA v1.0: kilometer-scale downscaling of an Australian regional atmospheric reanalysis over four midlatitude domains. *Geoscientific Model Development*, *14* (7), 4357–4378.

Swann, A., Hoffman, F., Koven, C. and Randerson, J. (2016). Plant responses to increasing $CO_2$ reduce estimates of climate impacts on drought severity. *Proceedings of the National Academy of Sciences, 113* (36), 10019-10024.

Tait, A. and Turner, R. (2005). Generating Multiyear Gridded Daily Rainfall over New Zealand. *Journal of Applied Meteorology*, *44* (9), 1315–1323.

Tait, A. and Woods, R. (2007). Spatial Interpolation of Daily Potential Evapotranspiration for New Zealand Using a Spline Model. *Journal of Hydrometeorology*, *8* (3), 430–438.

Tait, A., Sturman, J. and Clark, M. (2012). An assessment of the accuracy of interpolated daily rainfall for New Zealand. *Journal of Hydrology (NZ)*, *51* (1), 25–44.

Tootoonchi, F., Sadegh, M., Haerter, J., Räty, O., Grabs, T. and Teutschbein, C. (2022). Copulas for hydroclimatic analysis: A practice-oriented overview. *WIREs Water*, *9* (2), 1–28.

Wang, S, Yoon, J., Becker, E. and Gillies, R. (2017). California from drought to deluge. *Nature Climate Change, 7* (7), 465-468.

Whan, K., Zscheischler, J., Orth, R., Shongwe, M., Rahimi, M., Asare, E. and Seneviratne, S. (2015). Impact of soil moisture on extreme maximum temperatures in Europe. *Weather and Climate Extremes*, *9* (3), 57–67.

Wittwer, G. and Waschik, R. (2021). Estimating the economic impacts of the 2017-2019 drought and the 2019-2020 bushfires on regional NSW and the rest of Australia. *The Australian Journal of Agricultural and Resource Economics, 65* (4), 918-936.

Wu, H., Su, X., Singh, V., Feng, K. and Niu, J. (2021). Agricultural Drought Prediction Based on Conditional Distributions of Vine Copulas. *Water Resources Research*, *57* (8), 1–23.

Yang, Y., Uddstrom, M., Revell, M. and Moore, S. (2014). Soil moisture simulation by JULES in New Zealand: verification and sensitivity tests. *Meteorological Applications*, *21* (4), 888–897.

Zscheischler, J., Michalak, A., Schwalm, C., Mahecha, M., Huntzinger, D., Reichstein, M., Berthier, G., Ciais, P., Cook, R., El-Masri, B., Huang, M., Ito, A., Jain, A., King, A., Lei, H., Lu, C., Mao, J., Peng, S., Poulter, B., Ricciuto, D., Shi, X., Tao, B., Tian, H., Viovy, N., Wang, W., Wei, Y., Yang, J. and Zeng, N. (2014). Impact of large-scale climate extremes on biospheric carbon fluxes: An intercomparison based on MsTMIP data. *Global Biogeochemical Cycles*, *28* (6), 585–600.

Zscheischler, J., Van Den Hurk, B., Ward, P. and Westra, S. (2020). Multivariate extremes and compound events. In Stillmann, J., Sippel S. and Russo S. (Eds.), *Climate Extremes and Their Implications for Impact and Risk Assessment* (pp. 59–76). Amsterdam, Netherlands: Elsevier.

Zscheischler, J., Westra, S., van den Hurk, B., Seneviratne, S., Ward, P., Pitman, A., AghaKouchak, A., Bresch, D., Leonard, M., Wahl, T. and Zhang, X. (2018). Future climate risk from compound events. *Nature Climate Change*, *8* (6), 469–477.